2011

# INTERFERENCE EFFECTS IN RESTRICTED SYSTEMS

Swarbhanu Chatterjee
*University of Rhode Island*, swarbhanu77@gmail.com

# INTERFERENCE EFFECTS IN RESTRICTED SYSTEMS

BY

SWARBHANU CHATTERJEE

A DISSERTATION SUBMITTED IN PARTIAL FULFILLMENT OF THE

REQUIREMENTS FOR THE DEGREE OF

DOCTOR OF PHILOSOPHY

IN

PHYSICS

UNIVERSITY OF RHODE ISLAND

2011

DOCTOR OF PHILOSOPHY DISSERTATION

OF

SWARBHANU CHATTERJEE

APPROVED:

Dissertation Committee:

Major Professor Dr. Alexander Meyerovich

Dr. Sze Yang

Dr. Leonard Kahn

Dr. Gerard Muller

Dr. Nasser H. Zawia

DEAN OF THE GRADUATE SCHOOL

UNIVERSITY OF RHODE ISLAND

2011

## ABSTRACT

I considered two types of interference problems in restricted systems: the interference between bulk and boundary scattering in metal films and the effect of interference between particle repulsion and the constraining potential in Bose-Einstein Condensation (BEC) in inhomogeneous traps. The quantum mechanical and quasiclassical interference between bulk and boundary scattering in thin metal films with rough surface was first investigated by calculating the effective transport time beyond the Mathiessen's approximation, which was shown to exhibit a non-analytical dependence on the bulk relaxation time. The interference between the bulk and boundary scattering channels strongly affects the effective transport time and conductivity and is dependent on the temperature and the concentration of the impurities. Simple analytical expressions for the results for large bulk free paths $\mathcal{L}_b$ and large correlation radii (lateral sizes) $R$ of surface inhomogeneities were found. At $R^2 \sim a\mathcal{L}_b$ a crossover was predicted between two asymptotic regimes for interference contributions characterized by a different dependence to temperature and concentration. I also studied the condensation process in a strongly interacting trapped BEC in an optical lattice. The interaction between particles in a BEC within a trap pushes the normal particles to a spherical shell in the periphery reducing the condensation problem to a quasi-two dimensional one. By conducting a study of these two types of interference problems in different restricted systems, I was able to better understand the underlying physics of competing phenomena in these systems.

## ACKNOWLEDGMENTS

I am very grateful to my advisor, Dr. Alexander Meyerovich, for teaching me how to do physics and collaborating with me in research that led to publications. Without him, my dissertation would not have been possible. I am very glad that I have had the opportunity to learn how to do research by observing him. I am also very grateful to Dr. Peter Nightingale for interesting and helpful discussions during my research, and Dr. Leonard Kahn and Dr. Gerhard Muller for advice and support during my graduate studies. I am grateful to all my professors who through their discussions and courses helped me take the steps that led to my becoming a better researcher. I hope that I will be able to build on what I have learned during my PhD years and make myself a better worker and human being.

## DEDICATION

My parents, Tapan Chattopadhyay and Jaya Chattopadhyay, for continually encouraging me during long years to complete my PhD in physics. Even when we were geographically distant and could converse only by phone or email, they have been always present in who I am and everywhere I go. Without their support and advice, I would be much less compared to what I aspire to become as a human being and a professional.

## TABLE OF CONTENTS

**Page**

## LIST OF FIGURES

# CHAPTER 1

## Interference In Restricted Systems

### 1.1 Introduction

In the quantum world of tiny length scales or $\mu K$ temperatures where the quantum description is the only true description of systems, there are often different phenomena which compete with each other in trying to determine the equilibrium or non-equilibrium states of a system. The competition between rival mechanisms makes the system more interesting to study from a physicist's point of view. Often such systems are found to be in distinct regimes, which are regions in phase space where one mechanism predominantly decides the state and behavior of the system or where both mechanisms play an equal role.

For my thesis, I have considered two systems that are restricted in size: a thin metal film where the electron conductivity is influenced by both bulk impurities and surface roughness scattering; and a trapped atomic Bose-Einstein Condensate (BEC) with strong particle interactions. The fact that both systems are restricted to a small size, in atleast one of the spatial dimensions if not all three is important for different reasons in the two systems.

For a thin metal film, the thinness of the film quantizes one of the electronic state variables, the electron's momentum perpendicular to the film's plane, and increases the energy gaps of the bands and makes the system more quantum in nature. This has an important effect on the nature of the dependence of the conductivity on the electron scattering mechanisms in the film. I will show in this thesis how the quantum nature of the thin film causes an interference between bulk and the surface scattering channels because of which we cannot do what the Matthiessen's rule prescribes: regard the two scattering channels as independent mechanisms. I will also show how the system can exist in different regimes as far

as the nature of their conductivity is concerned depending on the mean free path and the correlation radius of the surface roughness.

In the other restricted system I have studied, i.e. a trapped atomic BEC with strong particle interactions, the nature of the condensation is strongly influenced by a competition between the trap that tries to confine the BEC and the particle interactions, which try to widen the condensate droplet. I have taken into account the shape of the wall in determining the particle wave functions after the droplet has already assumed a certain size. I achieved a self-consistent description of the system that takes into account all the competing mechanisms. I showed that because of self-consistency, the different mechanisms could not be treated independently and that the mechanisms had an interfering nature. This is in the very nature of a self-consistent description. Taking into consideration all the three mentioned mechanisms, the confining trap, the particle interactions and the nature of the particle wavefunctions up the wall of the trap, I found that after a condensate droplet of an initial size has already grown, the rest of the condensation happens in a manner that had not been previously described or explained as intuitively. The results obtained for the condensation behavior of such atomic BECs can be easily verified by experiments.

In the sections that follow, I analyze the interference in bulk and boundary scattering in thin metal films, after which I provide an analytcal description of the interference between competing mechanisms in a trapped and strongly interacting BEC. I then summarize my results.

## 1.2 Bulk and boundary scattering interference in thin metal films

With rapid advances in vacuum and low temperature technologies and in the field of material science, there have been many attempts at system miniaturization. Circuits and the metallic interconnects inside them have been made smaller

and researchers are making thinner and purer metal films to conduct electricity. When the thickness of these metal films becomes so small that it is comparable to the mean free path of the electrons in the metal, the boundary scattering becomes more important than the bulk scattering. In some experiments , surface roughness accounts for almost half of the overall resistivity of nanosystems [1]. The wall scattering involves an entangled combination of processes of different physical nature such as changes in energy spectra near the walls, stick-slip motion and partial accommodation, scattering by surface roughness and impurities, surface states, *etc.* Furthermore, the boundary and bulk scattering processes are no longer necessarily independent of each other but can interfere. Therefore, they cannot be treated independently and their effects on resistivity do not add up in a simple way. For example, when scattering is weak, as it is often the case for electron-phonon scattering or scattering by slight surface roughness, the establishing of mean free path requires several scattering events. These scattering events include the scattering off the rough walls. As a consequence, the transport properties become sensitive to the order of scattering events involving various channels. In clean metal films at not very low temperatures the main bulk channels are the electron-phonon scattering, scattering by grain boundaries and by residual impurities. I assumed that the films are pure and that the density of grain boundaries is relatively small and concentrate either on electron-phonon processes or on scattering by impurities. For surface scattering, I assumed that the main scattering effects result from scattering by surface roughness. One important goal was to see if the interference leads to an unusual dependence of the conductivity on the temperature or the impurity concentration which could be a signature of such interference. In addition, it was important to find a way of extracting parameters of surface roughness from the experimental data on conductivity.

The usual approach to transport in films is to use a collision operator in a transport equation to account for bulk scattering processes and to relegate all boundary scattering to a phenomenological boundary condition (one of the best-known examples of earlier work in this direction can be found in Refs. [2–5]). One then expresses the phenomenological parameters in this boundary condition (such as, for example, the specularity coefficient $p$ or the Namba [6] ratio of the amplitude of roughness and the mean free path, $\ell/\mathcal{L}_b$) via physical characteristics of surface. This approach has two issues associated with it. First, the choice of the *form* of the boundary condition by itself imposes limitations, which are not always clear on what kind of surface physics can or cannot be properly incorporated by this condition. Secondly, the bulk and surface scattering processes are accounted for within different mathematical frameworks - the former by the bulk collision operator and the latter as the boundary condition. Consequently, one should always expect certain entanglement between surface and bulk scattering in the transport results obtained this way and therefore, it is not always clear to what extent the emergence of non-Mathiessen's terms reflects real physical interference between different scattering processes and is not a mathematical artifact.

Recently, there appeared an alternative approach to boundary scattering which in clean systems can be dominated by the scattering by boundary roughness. This approach to roughness-driven transport is based on a mapping transformation technique, which in application to transport in ultrathin systems was developed in Refs. [7–9]. The approach involves mapping of a system with random rough boundaries onto an equivalent physical system with ideal boundaries but distorted bulk Hamiltonian. This allows one to incorporate the scattering by surface roughness inside the same collision operator as the bulk scattering processes. Though this is not the only approach to scattering by surface roughness (see a short review in the

second Ref. [10]), the mapping transformation is convenient for the simultaneous description of bulk and surface scattering by providing the uniform description of all scattering channels within the single mathematical formalism. As a result, this approach naturally covers the interference non-Mathiessen's terms (see the second Ref. [5, 7]). The mapping transformation approach allows one not only to develop a mathematically rigorous derivation for the bulk quantum transport equation and the collision operator, which reflects the boundary roughness in the initial problem, but also to understand the limitations and accuracy of alternative approaches to the problem [10, 11]. A somewhat similar, though technically different quantum approach based on the surface scattering model of Ref. [12] has been outlined in Refs. [13, 14] in the white noise approximation for a rough surface (see also the extension of this approach beyond the white noise in Ref. [15]). This approach corresponds to adding the surface scattering as a perturbation of the type [12] to the single-particle Green's function which already includes the bulk scattering. In diagrammatic language, this corresponds to adding a surface interaction line on top of the propagator averaged over the bulk interaction (bold line). Such an approach excludes from the outset all the diagrams with the intersecting bulk and surface interaction lines, which were included in Ref. [16], and, therefore misses some of the interference terms. Besides, the perturbative approach of Ref. [12], being, probably, the best and the simplest as long as it is justified, has a narrower application domain than the properly applied mapping transformation (see Ref. [10, 11]).

The mapping transformation provides a theoretical framework for transport formalism for systems with scattering channels of different nature. Since now bulk and surface scattering channels are treated in the same way, the results should reveal the full physical interference between bulk and surface scattering in transport.

Based on this approach, a rigorous diagrammatic derivation of the quantum transport equation for particles in quantized films with bulk and boundary scattering was developed in Ref. [16] . Though this approach is indeed rigorous and has a well-defined accuracy, the resulting equations are too complicated and difficult to use because of the interplay between numerous physical parameters and sources of interference.

In the following chapter, I show the results of the application of the quantum transport approach [16] to the non-Mathiessen's terms that arise from the quasiclassical interference between bulk and surface scattering by my collaborator and myself. For the quasiclassical case, the thickness of the film is large enough that the energy states of the electrons lie in bands. I also decribe how our results compared with the (scarce) experimental data on non-Mathiessen's contributions. I also compare our results with the Fuchs-Sondheimer equations [2, 4] and get the expression for the specularity coefficient via the roughness profile. In chapter 3, I describe the results obtained for a purely quantum calculation using the quantum transport equation to show the effects of surface-bulk interference on the resistivity. In chapter 4, I describe my study of the interference between particle interaction and the trap potential for a BEC, motivated by recent experiments on BEC in traps with or without optical lattice inside, in which the particles cannot be regarded as non-interacting. To underline the importance of the problem, it is worth mentioning that there have been three Nobel Prizes dedicated to the study of BEC. Our investigations provided an intuitive treatment of the problem of particle interaction in a BEC and its effects on the condensation process inside an optical trap. In chapter 5, I summarize our results on the nature of the surface-bulk interference in the resistivity for both the quantum and the quasiclassical cases and I compare it with the interference between particle interaction and trapping

potential in BECs trapped in an optical lattice.

### 1.2.1 The quasiclassical interference in a thin film

In ultrathin films, the motion across the film is quantized, $p_{zj} = \pi j\hbar/L$, where $L$ is the thickness of the film. This quantization, which is responsible for quantum size effect (QSE) in transport, leads to a splitting of the $3D$ spectrum $\epsilon(\mathbf{p}) = p^2/2m$ into a set of $2D$ minibands $\epsilon_j(\mathbf{q})$ where $\mathbf{q}$ is the component of momentum along the film [in the simplest case of parabolic spectrum with effective mass $m$, $\epsilon(\mathbf{p}) = p^2/2m$, the minibands are also parabolic, $\epsilon_j(\mathbf{q}) = (1/2m)\left[(\pi j\hbar/L)^2 + q^2\right]$]. Under certain realistic conditions, which have been analyzed in Ref. [16] in detail, the diagrammatic equations for the full single-particle Green's functions, which include both bulk and surface scattering, contains the following imaginary part in the energy denominator which we call the effective relaxation time $\tau_j^{(eff)}(\mathbf{q})$ for particles from each miniband $\epsilon_j(\mathbf{q})$ (*cf.* Ref. [13]):

$$\frac{1}{\tau_j^{(eff)}(\mathbf{q})} = \frac{1}{\tau_j^{(b)}(\mathbf{q})} + \sum_{j'=1}^{S} \int \frac{W_{jj'}(\mathbf{q},\mathbf{q}')/\tau_{j'}^{(b)}(\mathbf{q}')}{\left(\epsilon_{j'}(\mathbf{q}') - T_F\right)^2/\hbar^2 + \left(1/2\tau_{j'}^{(b)}(\mathbf{q}')\right)^2} \frac{d\mathbf{q}'}{(2\pi\hbar)^2}. \qquad (1)$$

Here $S$ is the total number of occupied or energetically accessible minibands $\epsilon_j(\mathbf{q})$, and $\tau_j^{(b)}(\mathbf{q})$ is the bulk relaxation time in each miniband $\epsilon_j$, which should be treated not as phenomenological parameter, but as an unambiguously defined imaginary part in the denominator of the single-particle Green's function for the unrestricted bulk. In our context, the bulk parameters $\tau_j^{(b)}(\mathbf{q})$ are determined by electron-phonon or impurity scattering in the bulk and are considered known. The wall-induced transition probabilities $W_{jj'}(\mathbf{q},\mathbf{q}')$ between the states $\epsilon_j(\mathbf{q})$ and $\epsilon_{j'}(\mathbf{q}')$ are determined by the correlation functions of surface inhomogeneities on both walls, $\zeta_{11}$ and $\zeta_{22}$, and by the interwall correlation of surface inhomogeneities $\zeta_{12}$, Ref. [11]. When the metal film can be treated as a $2D$ square well, the equations

for these transition probabilities are quite simple:

$$W_{jj'}\left(\mathbf{q},\mathbf{q}'\right)=\frac{\pi^4\hbar^2}{m^2L^6}\left(\zeta_{11}\left(\mathbf{q}-\mathbf{q}'\right)+\zeta_{22}\left(\mathbf{q}-\mathbf{q}'\right)+2\left(-1\right)^{j+j'}\zeta_{12}\left(\mathbf{q}-\mathbf{q}'\right)\right)j^2j'^2. \tag{2}$$

Though most of the calculations can be performed for any type of surface correlator, here we assume that the correlations of inhomogeneities on both walls are identical $\zeta_{11}=\zeta_{22}$ and Gaussian,

$$\zeta\left(\mathbf{s}\right)=\ell^2\exp\left(-s^2/2R^2\right),\ \zeta\left(\mathbf{q}\right)=2\pi\ell^2R^2\exp\left(-q^2R^2/2\hbar^2\right) \tag{3}$$

where $\ell$ and $R$ play the role of the amplitude (height) and correlation radius (lateral size) of surface inhomogeneities and that there are no interwall correlations, $\zeta_{12}=0$. [The Gaussian peak in the $\delta$-function limit $R\to 0$ corresponds to the white-noise correlations of Refs. [5, 7, 13]]. In practice, the correlation function of surface inhomogeneities is not always Gaussian (see Refs. [15, 17–19] and references within). However, there are reasons to believe that the exact profile of the correlation function becomes important qualitatively only for large-scale roughness, $R\gg L$ [20, 21].

The competing roles played by the bulk and surface scattering can be described by two dimensionless parameters, $t$ and $u$, the first of which characterizes the bulk scattering and the second - the correlation of surface roughness:

$$t=\tau_b\ p_F^2/m\ \hbar,\ u=p_F^2R^2/\hbar^2\sim R^2/a^2\geq 1, \tag{4}$$

where $p_F\sim\hbar/a$ is the Fermi momentum, $a$ is the atomic size.

For phonon scattering, all temperature dependence of the surface-bulk interference contributions to conductivity enter solely via parameter $t$. At high temperatures $T\gg\Theta_D$ the value of this parameter has the order of magnitude of [22, 23]

$$t\sim\frac{\tau_bT_F}{\hbar}\sim\frac{T_F}{T}\gg 1,\ \frac{t}{\sqrt{u}}=\frac{\tau_b\ p_F}{m\ R}\sim\frac{a}{R}\frac{T_F}{T}, \tag{5}$$

while at low temperatures $T \ll \Theta_D$

$$t \sim \frac{\tau_b T_F}{\hbar} \sim \frac{T_F}{\Theta_D}\left(\frac{\Theta_D}{T}\right)^3 \gg 1,\ \frac{t}{\sqrt{u}} = \frac{\tau_b\, p_F}{m\, R} \sim \frac{a}{R}\frac{T_F}{\Theta_D}\left(\frac{\Theta_D}{T}\right)^3, \tag{6}$$

where $\Theta_D$ is the Debye temperature. [There are experimental indications that $\Theta_D$ in ultrathin films depends on film thickness [24]]. At high temperatures, the ratio $t/\sqrt{u}$ is large or small depending on whether the lateral size of surface inhomogeneities is smaller or larger than approximately $10a$. At low temperatures this ratio is always large with the exception of surfaces with extremely long-range inhomogeneities such as in bent or non-uniformly stretched films with smooth surfaces. The transition between high- and low-temperature cases can be described by the usual extrapolation equations none of which is very reliable.

When impurity scattering is the main scattering mechanism in the bulk, parameter $t$ is temperature independent,

$$t \sim \frac{\tau_b T_F}{\hbar} \sim \frac{a^2}{c\sigma}, \tag{7}$$

where $c$ is the concentration of impurities and $\sigma$ is the scattering cross-section.

In general, the non-Mathiessen's contribution to the collision time $1/\tau_j^{(int)}$, which describes the interference between the bulk and surface scattering channels, can be defined as

$$\frac{1}{\tau_j^{(int)}(\mathbf{q})} = \frac{1}{\tau_j^{(eff)}(\mathbf{q})} - \frac{1}{\tau_j^{(b)}(\mathbf{q})} - \lim_{t\to\infty}\sum_{j'=1}^{S}\int \frac{W_{jj'}\left(\mathbf{q},\mathbf{q}'\right)/\tau_{j'}^{(b)}(\mathbf{q}')}{\left(\epsilon_{j'}\left(\mathbf{q}'\right)-T_F\right)^2/\hbar^2 + \left(1/2\tau_{j'}^{(b)}(\mathbf{q}')\right)^2}\frac{d\mathbf{q}'}{(2\pi\hbar)^2} \tag{8}$$

We cannot always use Eq. (1) directly for calculation of conductivity in ultrathin metal films due to two reasons. First, the observation of the full QSE effect in conductivity of metals is very difficult if not outright impossible. QSE in transport is associated with a saw-tooth dependence of the transport coefficients

on the film thickness, Refs. [8, 25]. In metals, the scale of these saw teeth is atomic and, to the best of our knowledge, there are very few observations of signs of such a saw-tooth dependence of the metal conductivity on $L$ [26, 27]. The reason is that the Fermi momentum in metals $p_F$ is of the order of $p_F \sim \hbar/a$ where $a$ is the atomic size. Then the parameter $p_F L/\hbar \sim L/a$ is usually large, the transport is quasiclassical, and the saw teeth too close to each other to be resolved. On top of that, the phonon collisions at not very low temperatures are rather robust, $\tau_b \Delta\epsilon_j/\hbar \sim (a^2/L^2)\,(T_F/\Theta_D)$, and can lead to a smearing of QSE. This all means that Eq. (1) in metals should be replaced by a similar quasiclassical equation. This transition from quantum to quasiclassical transport is fairly straightforward and requires replacement of summation over the miniband index $j$ by the integration over the continuous variable $p_x$, $\pi j\hbar/L \to p_x$. Such a transition in the framework of helium Fermi liquids has already been suggested in Refs. [28, 29]; for further applications see also Ref. [30]. As an additional benefit, the transition to the quasiclassical equations allows one to avoid dealing with atomistic peculiarities of the surface structure which lead to a reconstruction or even destruction of the Fermi surface near the surface in the ultra-quantum regime [31, 32].

The second reason for modification of Eq. (1) is the fact that this equation describes the two-channel collision time $\tau^{(eff)}$ (*i.e.,* the pole in the single-particle Green's function averaged over bulk and surface collisions) while the conductivity contains the effective *transport* time $\tau_{tr}^{(eff)}$ which is defined via the diffusion pole in the proper response function and, in our case, describes the single-particle diffusion/mobility or electric conductivity $\sigma$,

$$\sigma = \frac{e^2 \tau_{tr}^{(eff)}}{m^2} \int \sum_{j'=1}^{S} \delta\left(\epsilon_j - \epsilon_F\right)\; q_j^2 \frac{qdq}{4\pi\hbar^2},\; q_j^2 = p_F^2 - \pi^2\hbar^2/L^2. \tag{9}$$

Our effective transport time $\tau_{tr}^{(eff)}$ is not some phenomenological parameter but is an unambiguously defined quantity which describes the combined transport

effects of the two-channel scattering. To get the transport time $\tau_{tr}^{(eff)}$ and, therefore, the conductivity (9), one should solve the quantum transport equation with $\tau_j^{(eff)}(\mathbf{q})$, Eq. (1) , in the kernel of collision operator. [For exact quantum definition of the transport time $\tau_{tr}^{(eff)}$ via the irreducible bulk scattering vertex and the surface scattering probabilities $W_{jj'}(\mathbf{q},\mathbf{q}')$ see Ref. [16]]. This is a straightforward numerical task [16] only in the ultra-quantum case which involves a relatively small number of minibands $S$; in the quasiclassical limit with large $S$ the corresponding transport equation involves an extremely large number of minibands and requires inversion of huge matrices. Even for small $S$, one needs detailed information on bulk collision times $\tau_j^{(b)}(\mathbf{q})$ for each miniband. Since we do not have such information about *bulk* collisions, we are forced to simplify the equations and work with constant $\tau_j^{(b)}$.

An analysis similar to Ref. [28] indicates that a reasonable quasiclassical approximation for the transport time $\tau_{tr}^{(eff)}$ of Ref. [16] may be given by the quasiclassical equation

$$\frac{1}{\tau_{tr}^{(eff)}(\mathbf{p})}=\frac{1}{\tau_{tr}^{b}}+\frac{1}{\tau_b}\int\frac{W(\mathbf{p},\mathbf{p}')(1-\cos\gamma)}{(\epsilon(\mathbf{p}')-\mu)^2/\hbar^2+1/4\tau_b^2}\frac{d\mathbf{p}'}{(2\pi\hbar)^3}, \tag{10}$$

where $\gamma$ is the angle between the vectors $\mathbf{q}$ and $\mathbf{q}'$, the wall scattering rate is

$$W(\mathbf{p},\mathbf{p}')=\frac{4\pi}{L}\left(\frac{\ell R}{\hbar m}\right)^2 p_x^2 p_x'^2\exp\left(-(\mathbf{q}-\mathbf{q}')^2R^2/2\hbar^2\right), \tag{11}$$

and $\tau_{tr}^b$ and $\tau_b$ are the *bulk* transport and collision times. Simultaneously, the quantum equation (9) acquires the simple Drude-like form

$$\sigma=\frac{e^2 n\tau_{tr}^{(eff)}}{m}. \tag{12}$$

Eq.(10) becomes exact when the main contribution to lateral transport comes from the gliding electrons - electrons from the miniband with the smallest $p_x$ when the bulk collision time should be treated as $\tau_1^b$. In the limiting case of extremely large

bulk collision times, *i.e.*, at very low temperatures, the convergence of the integral (10) is ensured by the quantum cut-of $p_x = \pi\hbar/L$ rather than $1/\tau_b$ in denominator.

What we lose in such a transition from summation to integration is the quantum cut-off in transport that is responsible for capping the diverging contribution from gliding electrons to transport in high-quality low-temperature films. In sum (1) the minimal component of momentum perpendicular to the film is $\pi\hbar/L$ and the sum is always finite. The quasiclassical integral (10) , on the other hand, allows electrons to have zero normal component of momentum*, i.e.,* allows existence of perfectly gliding electrons that do not collide with the surface and, therefore, contribute disproportionately to transport. Another result of the lack of quantum cut-off is that the dependence of the surface contribution to effective transport time on the film thickness becomes trivial. More complex dependencies of the transport coefficients on $L$ in ultrathin high-quality films are almost invariably signs of the quantum cut-off and QSE.

At high temperatures $T \gg \Theta_D$ the electron-phonon transport and collision times, $\tau_{tr}^b$ and $\tau_b$, are roughly the same and differ from each other by an insignificant constant. A good estimate for $\tau_{tr}^b$ and $\tau_b$ can be obtained from the experimental data on bulk resistivity $\rho$ [23], $1/\tau_{tr}^b = n\ e^2\rho/m$. Using the data for Cu, $\rho\left(\theta_D\right) = 4.88 \times 10^{-8}\ \Omega m$, $n = 8.47 \times 10^{28}\ m^{-3}$, and $\epsilon_F = 7\ eV$ and assuming that $\tau_{tr}^b$ and $\tau_b$ are the same, one gets $t \simeq 173\ \left(\Theta_D/T\right)$. Similar estimate for Ag, $n = 5.86 \times 10^{28} m^{-3}$, $\rho\left(\theta_D\right) = 3.5 \times 10^{-8}\Omega m$, $\epsilon_F = 5.49\ eV$ yields $t \simeq 273\ \left(\Theta_D/T\right)$ meaning that cases $t$ is relatively large for both metals. At low temperatures $T \ll \Theta_D$ the bulk transport and collision times are markedly different, $\tau_{tr}^b \sim \left(\Theta_D/T\right)^2 \tau_b \gg \tau_b$. In the case of impurity scattering the difference between $\tau_{tr}^b$ and $\tau_b$ is less pronounced.

### 1.2.2 The quasiclassical effective transport time

We now give simple estimates for the effective transport time (10) . Introducing new variables as

$$\begin{aligned} p_x &= p_F \cos\theta,\ q = p_F \sin\theta,\ p'_x = x p_F \cos\phi, \\ q' &= x p_F \sin\phi,\ n = p_F^3/3\pi^2\hbar^3 \end{aligned} \tag{13}$$

one can reduce the effective transport time (10) to a dimensionless integral

$$\begin{aligned} \frac{1}{\tau_{tr}^{eff}} &= \frac{1}{\tau_{tr}^{b}} + \frac{12T_F}{\pi\hbar}\frac{\ell^2 R^2 n}{L}\frac{1}{t}\int_0^\pi d\theta\cos^2\theta\int_0^\infty x^4 dx\int_0^\pi d\phi\int_0^{2\pi} d\gamma \\ &\times\frac{\cos^2\phi\sin\phi e^{-\frac{u}{2}\left(\sin^2\theta+x^2\sin^2\phi-2x\sin\theta\sin\phi\cos\gamma\right)}\left[1-\cos\gamma\right]}{\left[\left(x^2-1\right)^2+\frac{1}{t^2}\right]}. \end{aligned} \tag{14}$$

After integration over $d\gamma$, the transport time reduces to

$$\frac{1}{\tau_{tr}^{eff}} = \frac{1}{\tau_{tr}^{b}} + \frac{T_F}{\hbar}\frac{\ell^2}{L\lambda_F}U(u,t), \tag{15}$$

$$\begin{aligned} U(u,t) &= \frac{16u}{\pi}\int_0^\pi d\theta\cos^2\theta e^{-\frac{u}{2}\left(\sin^2\theta+1\right)}\int_0^\infty dy y^4 e^{-\frac{u}{2}\left(y^2-1\right)} \\ &\times\left[I_0(uy\sin\theta)-I_1(uy\sin\theta)\right]F_1(y,t), \end{aligned} \tag{16}$$

$$F(y,t) = \frac{1}{t}\int_0^\pi d\phi\frac{\cos^2\phi}{\left[\left(y^2-\sin^2\phi\right)^2+\sin^4\phi/t^2\right]},.$$

where we replaced $x$ by $y = x\sin\phi$.

We note here that all the information about quasiclassical interference between surface and bulk scattering is contained in the function $U(u,t) - U_0(u)$ where $U_0(u) = U(u, t\to\infty)$. This function is plotted in Figure 1 as a function of $t$ for three different values of $u$, $u = 1; 10; 10$, while the function $U_0(u)$ is plotted in Figure 2. It is clear from the plot that the interference contribution decreases with increasing $t$ and with increasing correlation radius of surface roughness $R$ (with increasing $u$). For high quality films with large bulk mean free paths for which $t$ is large, $t \gg 1$, it is possible to obtain a relatively simple semi-analytical description

of $U(u,t)$ as an expansion in $1/t$. Note that $U(u,t)$ is not a regular function of $1/t$ and the expansion is, strictly speaking, in the powers of $1/\sqrt{t}$.

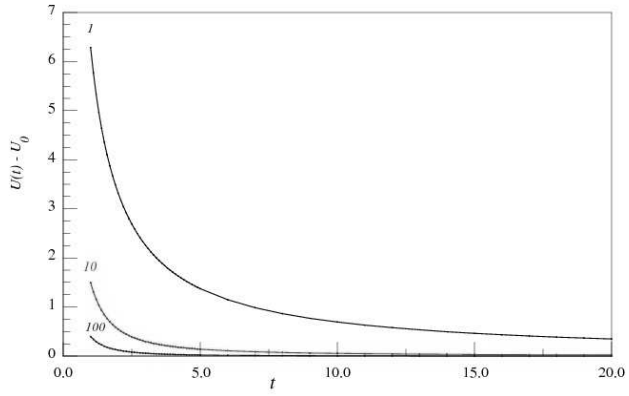


Figure 1. The interference contribution with varying $u$

As one can see, the integrals $(14), (15)$ are rather cumbersome. To better understand the results below one should keep in mind that at large $t$ and $u$ the integrand in is a product of two peaks one of which is a function of $t$ and the other - a function of $u$.

We note that the first peak is explained by a relatively large value of the electron-phonon collision time $\tau_b$ in clean metals at not very high temperatures and, therefore, by the large value of the dimensionless parameter $t \gg 1$. Function $F(y, t \to \infty)$ has singularities at $y \to 0$ and $y \to 1$. The former singularity is not dangerous because of the factor $y^4$ in the integrand. The latter one is eliminated by the factor $1/t$ in front of the integral. The peak in $y^4 F(0 < y < 1, t \to \infty)$ is asymmetric and is rather broad. From the physics standpoint, this asymmetry reflects the higher contribution to lateral transport from the gliding electrons with momenta almost parallel to the film surface. Function $y^4 F(0 < y < 1, t \to \infty)$

gradually increases when $y$ increases from 0 to 1 and rapidly drops almost to zero again when $y$ start approaching 1. At large $t$ the shape and parameters of this peak practically do not depend on $t$ except for a very narrow region near 1 in which $1-y^2 \sim 1/t$. At $y>1$, function $F(y, t\to\infty)$ remains small.

On the other hand, the peak of the integrand as a function of $y$ at $u \gg 1$ (or, more precisely, at $\sqrt{u} \gg 1$) represents a narrow peak of the width $1/\sqrt{u}$. At $\sqrt{u} \gg 1$ the the integrand in Eqs. (15) can be simplified using the asymptotic expressions for the Bessel functions,

$$I_{0,1}(z \gg 1) \sim e^z/\sqrt{2\pi z}, \tag{17}$$

which makes the integrand look like a Gaussian function,

$$e^{-\frac{u}{2}(y-\sin\theta)^2}, \tag{18}$$

and in the limit $u\to\infty$ - almost like a $\delta$-function,

$$y^4 e^{-\frac{u}{2}\left(y^2-1\right)}\left[I_0(uy\sin\theta) - I_1(uy\sin\theta)\right] \to \frac{1}{u} y^3 e^{u\left(\sin^2\theta+1\right)/2}\delta(y-\sin\theta). \tag{19}$$

This peak in the integrand at $\sqrt{u} \sim R/a \gg 1$ is explained by a small momentum transfer $\delta q \sim \hbar/R$ in scattering by smooth inhomogeneities with large lateral size $R$.

Integration over $d\phi$ in Eq. (15) yields the following expression for $F(y,t)$:

$$F(y,t) = \frac{\pi}{\sqrt{2}y^3} \frac{1/t}{\left[\sqrt{\left(y^2-1\right)^2 + \frac{1}{t^2}} + \left(y^2-1\right)\right]^{1/2}}. \tag{20}$$

The singularity at $y=0$ is eliminated by the extra factor $y^4$ (or, rather, $y^{7/2}$ because of the Bessel functions (17)) in the integrand in Eq. (15). Everywhere between $0<y<1$, except for points very close to $y=1$,

$$F(0<y<1, t\to\infty) \simeq F_0(y) = \frac{\pi}{2y^3}\sqrt{1-y^2}. \tag{21}$$

Corrections to this equation are of the order of $1/t^2$,

$$\frac{\pi}{8t^2y^3}\frac{1}{(1-y^2)^{3/2}}, \tag{22}$$

except for a very narrow region $y \to 1$.

At $y > 1$, but again not very close to $y = 1$, the main term in the function $F(y, t \gg 1)$ is of the order of $1/t$ and is, therefore much smaller than (21):

$$F_1(y > 1, t \gg 1) \simeq F_1(y) = \frac{1}{t}\frac{\pi}{2y^3}\frac{1}{\sqrt{y^2-1}}. \tag{23}$$

The contribution from this region to the integral over $dy$ is usually small, especially at $u \gg 1$ since the corresponding integral is also exponentially small in $u$.

Function $U(u, t \gg 1)$ is not an analytical function of $1/t$. Close to the point $y = 1$, *i.e.,* when $1/t \gg |1 - y^2|$, function $F_1(y \to 1, t \gg 1)$ behaves as $1/\sqrt{t}$ on both sides of $y = 1$,

$$F(y \to 1, t \gg 1) \to \frac{\pi}{\sqrt{2t}}. \tag{24}$$

Since the width of this region is approximately $1/t$, its contribution to the integral is of the order $1/t^{3/2}$. To find this non-analytical contribution one can keep only the main term in $(y - 1)$ in $F(y, t)$,

$$\widetilde{F}(y < 1, t) = \frac{\pi}{\sqrt{2}}\frac{1/t}{\left[\sqrt{4(y-1)^2 + \frac{1}{t^2}} + 2(y-1)\right]^{1/2}}, \tag{25}$$

and put $y = 1$ into all coefficients in front of $F$. The remaining integral,

$$\int_0^1 \widetilde{F} dy,$$

can be evaluated exactly. The main non-analytical contribution from this term is $1/\left(3\sqrt{2}t^{3/2}\right)$. To get the non-analytical contribution from the region $y > 1$, one should cut-off the corresponding integral at some large value $A$. The exact value of the cut-off $A$ is, of course, irrelevant for the non-analytical contribution from

the area close to $y = 1$ which turns out to be $-1/\left(3\sqrt{2}t^{3/2}\right)$. Therefore, the term $1/t^{3/2}$ disappears from the function $U(u, t \gg 1)$ and the first non-regular term in the expansion of the function $F$ in $1/t$ has the order $1/t^{5/2}$. The latter term is not important in our context.

Summarizing, at $t \gg 1$ the leading terms in the expansion of $U(u, t \gg 1)$ in $1/t$ are

$$U(t \gg 1, u) \simeq U_0(u) + \frac{1}{t}U_1(u) + \frac{1}{t^2}U_2(u) \tag{26}$$

with $U_0(u)$ coming from Eq. (21), $U_1(u)$ coming from Eq. (23), and $U_2(u)$ - from Eq. (22). Functions $U_0(u), U_1(u), U_2(u)$ are plotted in Figure 2.

The analytical expression for $U_0(u)$ is

$$U(u, t \to \infty) \equiv U_0(u) \tag{27}$$

where,

$$\begin{aligned} U(u, t \to \infty) &= 16u \int_0^\pi d\theta \cos^2\theta e^{-\frac{u}{2}\left(\sin^2\theta+1\right)} \int_0^1 \sqrt{1-y^2} y dy \; e^{-\frac{u}{2}\left(y^2-1\right)} \\ &\quad \times [\, I_0(uy\sin\theta) - \; I_1(uy\sin\theta)]\,. \end{aligned} \tag{28}$$

This function can be simplified at $u \gg 1$ using Eq. (19):

$$\begin{aligned} U_0(u \gg 1) &\simeq 16\sqrt{2\pi u} \int_0^\pi d\theta \sin\theta |\cos^3\theta| \left[\, I_0\left(u\sin^2\theta\right) - \; I_1\left(u\sin^2\theta\right)\right] / e^{u\sin^2\theta} \\ &= 16\sqrt{\frac{2\pi}{u}}. \end{aligned} \tag{29}$$

The result indicates that when the lateral size of surface inhomogeneities $R$ becomes bigger and the walls smoother, the wall-driven transport time increases proportionally to $1/R$. This term gives the pure surface contribution to transport.

The next terms in the expansion in $1/t$ are responsible for the surface-bulk interference in transport beyond the Mathiessen's rule. The first such term is

$$U_1(u) = 8u \int_0^\pi d\theta \cos^2\theta e^{-\frac{u}{2}\left(\sin^2\theta+1\right)} \int_1^\infty dy \; \frac{y}{\sqrt{y^2-1}} e^{-\frac{u}{2}\left(y^2-1\right)} \tag{30}$$

$$\times \left[I_0(uy\sin\theta) - I_1(uy\sin\theta)\right]. \tag{31}$$

At large $u$ this function behaves as $1/u^{3/2}$. More accurately,

$$\begin{aligned} U_1(u \gg 1) &\simeq \frac{8\ u}{2\sqrt{2\pi}} \int_0^\pi d\theta \cos^2\theta e^{-u\sin^2\theta/2} \int_1^\infty dy \frac{y}{\sqrt{y^2-1}} \frac{e^{-u\ y^2/2} e^{yu\sin\theta}}{(yu\sin\theta)^{3/2}} \\ &\simeq \frac{10}{u^{3/2}} \sqrt{\frac{2}{\pi}} \end{aligned} \tag{32}$$

(the last equation is a result of a numerical evaluation rather than of the exact analytical calculation of the integral). This also means that at $u \gg 1$

$$U_1/U_0 \to 5/(8\ \pi\ u) \tag{33}$$

and the contribution from $1/t$ becomes less and less significant with increasing lateral size of surface inhomogeneities $R$.

The computation of $U_2(u)$ is more cumbersome. This function comes from the integration over $dy$ from 0 to 1. To get this function, one should subsectiontract from the correspondent integral not only the zeroth-order term $F_0$, but also the terms that yield the $1/t^{3/2}$contribution:

$$\begin{aligned} U_2 &= 16u \lim_{t\to\infty} t^2 \int_0^\pi d\theta \cos^2\theta e^{-\frac{u}{2}\left(\sin^2\theta+1\right)} \int_0^1 dy \\ &\times \left[ \begin{array}{c} f(y)\left(F - F_0 - \widetilde{F} + \widetilde{F}_0\right) + (f(y) - f(1))\left(\widetilde{F} - \widetilde{F}_0\right) \\ +f(1)\left(\widetilde{F} - \widetilde{F}_0 - \frac{1}{3\sqrt{2}t^{3/2}}\right) \end{array} \right], \\ f(y) &= y^4 e^{-\frac{u}{2}y^2} \left[\ I_0(u\ y\ \sin\theta) - \ I_1(u\ y\ \sin\theta)\right], \\ \widetilde{F}_0 &= \frac{\sqrt{2}\pi}{y^3}\sqrt{1-y}. \end{aligned} \tag{34}$$

It is clear from Figure 2 that $U_2(u) \gg U_1(u)$ at $u \gg 1$. The reason is quite simple. At large values of $u$ the coefficients in front of $F$ in the integral over $dy$ form an almost Gaussian peak around some value of $y < 1$. Therefore, $U_2(u)$, which originates from the integral over $dy$ from 0 to 1, always dominates at $u \gg 1$ over $U_1(u)$, which originates from the integral from 1 to $\infty$. As a result, the term $U_2(u)/t^2$ in the expansion (26) of $U(u, t \gg 1)$ over $1/t$ can remain much

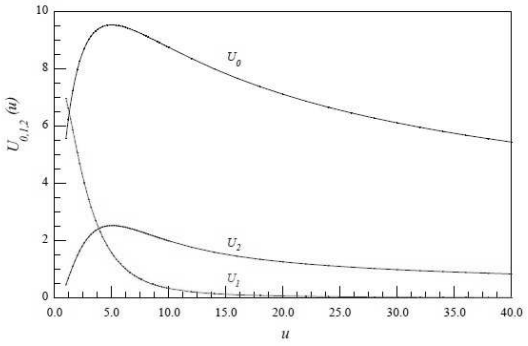


Figure 2. The functions $U_{0,1,2}(u)$.

larger than $U_1(u)/t$ even at large values of $t$. The crossover from $U_2(u)/t^2$ to the asymptotic behavior $U_1(u)/t$ occurs only when $t$ exceeds some critical value $t_{cr}$,

$$t_{cr}(u) = U_2(u)/U_1(u). \tag{35}$$

Function $t_c(u)$ is plotted in Figure 3. At relatively small values of $u$ (for practical purposes, at $u \leq 10$), $t_c$ is quadratic in $u$, $t_{cr} \approx 0.1u^2$. At larger values of $u$ (numerically, at $u \geq 15$), $t_c$ is linear in $u$, $t_c \approx u$. We can prove from analyzing the asymptotic behavior of $U_2(u)$ and $U_1(u)$ at $u \gg 1$ that $U_2(u) \propto 1/u^{1/2}$ and $U_1(u) \propto 1/u^{3/2}$ and, therefore, $t_c$ is indeed linear in $u$. However, we cannot prove that the proportionality coefficient is exactly 1. Numerically, this coefficient is approximately 0.99 though the accuracy of computation for Eq. (34) is limited by the presence of non-analytical term $1/t^{5/2}$. In the end, the assumption $t_c(u \gg 1) = u$ is sufficiently good for any potential comparison with experiment.

Summarizing, in high quality films with $t, u \gg 1$

$$U(t \gg 1, u \gg 1) \simeq \frac{10}{\pi}\sqrt{\frac{2\pi}{u}}\left(\frac{8\pi}{5} + \frac{1}{tu} + \frac{1}{t^2}\right) \tag{36}$$

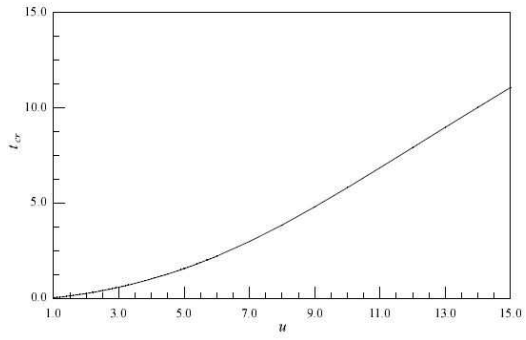


Figure 3. The function $t_{cr}\,(u)$.

or in normal variables

$$\frac{1}{\tau_{tr}^{eff}} \simeq \frac{1}{\tau_{tr}^{b}} + \frac{10\sqrt{2}}{\sqrt{\pi}} \frac{T_F}{p_F \lambda_F} \frac{\ell^2}{RL} \left( \frac{8\pi}{5} + \frac{\hbar}{2\tau_b\, T_F} \frac{\lambda_F^2}{R^2} + \frac{\lambda_F^2 m}{2\tau_b^2 T_F} \right). \tag{37}$$

This simple equation describes the asymptotic behavior of the wall contribution to conductivity of films (15) in the classical approximation. The crossover from $1/\tau_b$ to $1/\tau_b^2$ behavior of the interference term occurs at $R^2 \sim a\mathcal{L}_b$.

It could be instructive to compare the pure wall term in Eq. (37) with the Fuchs-Sondheimer result for the resistivity $\rho$,

$$\rho = \rho_b \left( 1 + \frac{3\mathcal{L}_b}{8L} \left( 1 - p \right) \right). \tag{38}$$

The comparison yields the following expression for the specularity coefficient $0 \leq p \leq 1$,

$$p = 1 - \frac{64}{3}\sqrt{2\pi}\, \frac{\ell^2}{\lambda_F R} \tag{39}$$

meaning that the Fuchs boundary condition can emulate scattering by rough surfaces only for a very small amplitude of roughness, $\ell^2 \ll \lambda_F R$. This this restriction is noticeably stronger than restriction on our approach [11] $\ell \ll R, L$. Of course,

the Fuchs-Sondheimer Eq. (38) does not contain the interference terms which represent the main thrust of this paper. Note that, in principle, the Fuchs boundary condition, which assumes partial accommodation by the perfect flat walls, does not have to emulate the results of locally specular scattering by rough walls for which the mean free path is established by the randomization of lateral momentum due to a series of reflections from randomly directed walls.

### 1.2.3 Accuracy of the results

I would like to now comment on the accuracy of our predictions and on ways for improvements. Though some of these potential improvements could seem rather straightforward, the others might require us to introduce new parameters, which, in turn, could make the results useless for any meaningful comparison with experiment. Below I will list some of the restrictions on the accuracy of our results and describe the ways of lifting these restrictions.

### 1.2.4 Accuracy of the main quasiclassical equations

Our results are based on a thorough diagrammatic derivation of the transport equation in films with bulk and roughness scattering channels in Ref. [16]. As it is shown in Ref. [16], the effective relaxation time $1/\tau_j^{(eff)}(\mathbf{q})$ reduces after averaging over surface roughness and bulk scattering to two diagrams for the self-energy function. The first one leads directly to Eq. (1) while the second one is disregarded following Ref. [16]. This is a common approximation used, in different forms, in most of the Green's function based transport derivations (see, *e.g.*, Refs. [13, 33] and references therein). This approximation is well justified when the bulk interaction has a short range which is usually the case for impurity scattering. For phonon scattering it might not work as well at very low temperatures.

In principle, we can add this disregarded second diagram to the equation for

the pole of the single-particle Green's function (1). However this would lead to a loss of transparency of the results and make any meaningful comparison with experiment virtually impossible: this diagram contains integrals with the full irreducible bulk vertex function, which is unknown and does not reduce to observables.

More worrisome is the heuristic transition from the quantum Eq. (1) for the relaxation time to the quasiclassical Eq. (10) for the transport time. This transition allowed us avoid inverting huge matrices stemming from the transport equation and get the quasiclassical results in a very compact analytical form. This is justified when the dominant contribution to transport comes from gliding electrons which are contained in the lowest quantum miniband and when the pure wall scattering dominates over the interference terms. We plan to revisit this issue in more detail later on.

### 1.2.5 Non-Gaussian correlations

In order to obtain the above results, we have assumed that the correlation function of surface roughness has a Gaussian form, Eqs. (1) − (3). Though the Gaussian correlations are practically universally used for theoretical description of rough surfaces, there is experimental evidence the correlations are sometimes non-Gaussian (see *,e.g.,* Refs. [17–19]). The difference between transport properties of *quantized* films with various types of surface correlations could be quite noticeable, especially for relatively smooth surfaces with $R \gg a$ which can exhibit, depending on the type of the correlation function, a new type of quantum size effect, Refs. [20, 21]. In the case of quasiclassical transport the difference is less striking and is easy to analyze. For example, the change in the correlation function lead to a replacement of the Gaussian factor in the integrand $W$, Eq. (11), by some other exponential or power-law function, which properly reflects the correlations, and results in a different power in the dependence $U(u)$. Numerically

this is a straightforward matter. The semi-analytical comparison between different roughness profiles will be done in a separate paper.

### 1.2.6 Surface-driven deformations

In our description of transport we assumed that the main transport effect of surface roughness is the scattering by surface inhomogeneities that reflect randomness in the position and direction of the surface. As a result, the transport parameters depend solely on the geometry of the surface, *i.e.,* the correlation function of surface roughness, and do not take into account the change in electron or phonon properties near the surface. Of course, the proximity to the surface leads to deformations inside the film, which affect the electron properties via the deformation potential. The deformation potential near surface inhomogeneities, especially near the ones with large curvature, changes the scattering parameters and makes the effective averaged cross-section different from the purely geometry-driven one. We discussed the ways to incorporate this effect into our formalism in Refs. [11]. Essentially, this is equivalent to the replacement of the scattering probability (11) by an effective function with similar symmetry. This resembles the description of transport in systems with bulk impurities in which the impurity scattering potential $U(\mathbf{r})$ is replaced by the effective $T$-matrix $T(\mathbf{p}, \mathbf{p}')$. Though this is the right way of dealing with the complications stemming from the surface-driven deformations, the *experimental* implications are not very appealing. The correlation function of surface roughness $\zeta(\mathbf{q})$ can be measured directly by scattering experiments, scanning surface microscopy, *etc.* This information is sufficient for direct application of our results without any unknown fitting parameters. If, on the other hand, the deformation potential near the surface is strong, one is forced to treat $W(\mathbf{p}, \mathbf{p}')$ as an effective average scattering cross-section. This inevitably leads to an appearance of fitting parameters and makes the results more ambiguous.

Another issue is the softening of phonon spectrum and, therefore, lowering of the Debye temperature near the surface [24]. When this effect is strong, the "bulk" scattering parameters that enter our non-Mathiessen's terms may differ considerably from their true bulk values.

### 1.2.7 Quantum size effect (QSE)

One of the main features of our results is the $1/L$ dependence of the wall contribution to the effective transport time $1/\tau_{tr}^{(eff)}$ on the film thickness which is consistent with the quasiclassical Fuchs-Sondheimer theory. In ultraclean films at very low temperatures, *i.e.*, at $t \to \infty$, the contribution from the gliding electrons should be cut-off not by $i/t$ in the pole of the integrand, but by the quantum cut-off, $p_x, p_x' > \pi\hbar/L.$,

$$\frac{1/\tau_b}{\left(\epsilon\left(\mathbf{p}'\right)-\mu\right)^2/\hbar^2 + 1/4\tau_b^2} \to 2\pi\delta\left(\epsilon\left(\mathbf{p}\right)-\mu\right), \tag{40}$$

$$\frac{1}{\tau_{tr}^{(eff)}} = \frac{1}{\tau_{tr}^{b}} + 2\pi \int_{p_x'>\pi\hbar/L} W\left(\mathbf{p}_F, \mathbf{p}'\right) \delta\left(\epsilon\left(\mathbf{p}\right)-\epsilon_F\right) \frac{\left(1-\cos\gamma\right) d\mathbf{p}'}{\left(2\pi\hbar\right)^3}. \tag{41}$$

Apart from ensuring the low-temperature cutoff, Eq. (41) also makes the dependence of the lateral conductivity $\sigma$ on the film thickness $L$ much more complicated than in Section 3 leading, for example, to $1/L^2$ [10, 11, 20, 21, 30] or $1/L^3$ dependence [10–12]. This more complicated wall contribution to the effective transport time $1/\tau_{tr}^{(eff)}$ than $1/L$ in experiment might be a direct sign of quantum size effects in transport. An even more accurate account of the quantum size effect would require us to return to summation, Eq. (1), instead of integration and to a saw tooth dependence of the conductivity on the film thickness $L$ which is similar to the one of Ref. [16] and is a common feature of QSE in films irrespective of the scattering channel [8, 10, 11, 25]. However, in metals the width of these saw teeth

is about atomic size $a$ and the observation of this type of dependence $\sigma(L)$ highly unlikely. We plan to study the effect of the quantum cut-off on the quasiclassical effective transport time separately.

### 1.2.8 The momentum dependence of the bulk relaxation time

The discussion above ignores the quantization of phonons in ultrathin films and, even more importantly, the momentum dependence of the bulk relaxation time $\tau_b(p_x, \mathbf{q})$ in Eq. (1). Not much is known about this function that can be useful in our context. Though one can easily write the formal expressions for $\tau_b(\mathbf{p})$ (see, for example, Refs. [22, 23] and numerous other publications), these expressions do not reduce to a set of observables which are independently known from experiment. In the end, any attempt to make our results more accurate by introducing the dependence $\tau_b(\mathbf{p})$ into the calculations would leave us with a large additional set of fitting parameters that would only obscure our understanding of surface contribution to transport in films.

The only real improvement could be achieved for ultrathin films at very low temperatures for which we should replace the averaged bulk experimental value $\tau_b$ used above by the corresponding constant for the gliding electrons $\tau_b(\pi\hbar/L, \mathbf{q}_F)$ - when this constant is known experimentally. The next step in the same directions could be the use of quantized - ultimately, two-dimensional - phonons. This will lead to an obvious change in the temperature dependence of the results.

### 1.2.9 Localization and related quantum interference phenomena

Above we deliberately ignored the roughness-driven localization of electrons. The localization length in quasi-twodimensional films with weak roughness is exponentially large and can manifest themselves only for the ultrathin films. Localization corrections within our formalism are discussed in detail in the first of

Refs. [11] which also contains references to earlier publications on localization and quantum interference effects associated with the surface disorder.

### 1.2.10 Discussion of the quasiclassical interference

The most interesting part of our results for the quasiclassical interference between bulk and surface scattering channels in electron transport in thin films is our simple asymptotic expression (37) for high quality films with large bulk free path $\mathcal{L}_b$ (*i.e.*, large $t$) and large lateral size of surface inhomogeneities $R$ (*i.e.*, large $u$). We do not know of past publications with such a simple and easily verifiable result. This result includes a crossover between two different asymptotic behaviors of the resistivity at $\mathcal{L}_b \sim R^2/a$. Irrespective of the bulk scattering channel, the crossover in the interference part of the resistivity can be observed as a change in its dependence on the correlation length (lateral size) of surface inhomogeneities $R$ from $1/R^3$ to $1/R$. Experimentally this crossover can manifest itself also as a change in the temperature (phonon scattering) or concentration (impurity scattering) dependencies of the resistivity. Note, however, that when $1/ut$ term in the interference contribution (36), (37) dominates over the $1/t^2$ term, the temperature/concentration dependence of the interference contribution is exactly the same as for the bulk term and the only distinguishing feature of the interference contribution is its $1/R^3$ dependence on $R$. Of course, when $1/t^2$ term dominates, the temperature/concentration dependence of the interference contribution is quite distinct from the main surface term.

Inspite of many decades of experiments on conductivity of ultrathin films, there are few data sets on the functional behavior of the interference between bulk and roughness-driven scattering. The experimental difficulties are mainly about ensuring that roughness is the main boundary scattering channel and maintaining the same surface roughness while manipulating the bulk properties. Currently, we

are aware of only one group which does measurements of the interplay between electron-phonon and roughness scattering channels as a function of temperature while simultaneously analyzing the surface roughness [19, 34].

It is instructive to compare our semi-analytical quasiclassical results with previous quantum computations which explicitly include QSE [7, 8, 13, 16]. Refs. [7] do not contain any explicit equations for the interference terms that can be compared with our results, especially in the quasiclassical regime. The authors of Ref. [8] were not interested in the interference terms and considered bulk and roughness scattering as two independent additive channels. Ref. [13] also does not contain any explicit information about the interference terms except for mentioning that these contributions seem to be smaller than the pure wall or bulk terms. In addition, Refs. [7, 8, 13] use the $\delta$-type (white noise) approximation for the surface roughness and, therefore, would not be able to see the crossover between interference regimes even if there were analytical results for the surface-bulk interference.

In our earlier computations of Ref. [16] we characterized the interference term by a dimensionless parameter $\Lambda$ which described the ratio of pure wall and bulk-wall interference contributions to the effective relaxation (or transport) time or the resistivity (12),

$$\Lambda = 1 + \frac{\tau^w}{\tau^{int}}.$$

In our notations,

$$\Lambda = \frac{U\left(t,u\right)}{U\left(t\to\infty,u\right)}.$$

For high-quality clean films (36) this ratio acquires the simplest form,

$$\Lambda = 1 + \frac{5}{8\pi}\left(\frac{1}{tu} + \frac{1}{t^2}\right) \tag{42}$$

and the correction to the limiting value $\Lambda = 1$ is positive.

The result (42) can be compared with the QSE dependence of $\Lambda$ on the bulk free path $\mathcal{L}_b$, $\Delta\left(p_0\mathcal{L}_b\right)$, in Ref. [16] ($p_0\mathcal{L}_b$ in [16] is equivalent to our $2t$). As it is clear from figures in Ref. [16], the correction to the limiting value $\Lambda = 1$ can be positive or negative, depending on the number of quantum minibands involved though it tends to become more negative with an increase in the number of minibands (increase in film thickness). Also, the deviation of $\Lambda$ from 1 in quantum case seems to increase with increasing $R$ (*i.e.*, with increasing $u$). It is not clear why the results of the same approach in quantum and classical limits are so different. One of the reasons could be the above mentioned heuristic transition from Eq. (1) to Eq. (10) in which we averaged the transport time over all minibands while structuring the result closer to discrete equations of Ref. [16] for the lowest minibands which contain the gliding electrons.

In experiments [19, 34] the correction to $\Lambda = 1$ seems to be negative (the corresponding term in resistivity $\Delta\rho$ decreases with increasing temperature). Though it is impossible to make a quantitative comparison with our results, qualitatively we tend to interpret these results as an experimental manifestation of QSE. There is one caveat. The experimental values of $\rho\left(T\right)$ is very close to the pure bulk values $\rho_b\left(T\right)$ and the functional behavior of both functions is almost very similar. One cannot discount the possibility that the surface-driven softening of the phonon modes and the renormalization of the Debye temperature should require the use a renormalized function $\widetilde{\rho}_b\left(T\right)$ rather than the true bulk function $\rho_b\left(T\right)$ as the basis for extracting $\Delta\rho$ from experiment [24]. If the mode softening is sufficiently strong, the extracted values of $\Delta\rho$ will actually increase with increasing temperature and exhibit the temperature dependence consistent with our $1/t$ dependence of the interference terms.

The dependence on the film thickness $L$, $1/\tau^{int}\left(L\right)$, in Ref. [16] starts, if one

disregards the inevitable QSE saw teeth, from the ultra-quantum form $1/L^6$ and shifts to $1/L^3$ in thicker films and finally to $1/L$ in thick films with dominant higher minibands. This behavior is consistent with our current results which yield the $1/L$ dependence without the quantum cutoff and higher powers when this cutoff becomes essential, Eq. (41). This also tells us that more often than not one should not expect a clear-cut power law in experimental dependence of resistivity on $1/L$. Accordingly, experimental data on the dependence of the resistivity on $1/L$ are inconclusive. One of additional artifacts is the potential presence of grain boundaries that can distort the roughness contribution if the films are not properly annealed as it has been recently demonstrated in Ref. [35]. Some of the recent experimental data have been summarized in Ref. [34]. This summary also does not lead to any definite conclusion on the power in the dependence of resistivity on $1/L$. Recent experimental results of Ref. [36] yield the dependence $1/L^{1.2}$ which is consistent with our results though the number of experimental points is relatively small to make a definite conclusion. As it was mentioned before, a higher power of $1/L$ in experimental data on the dependence of resistivity on film thickness for ultrathin films should be considered as a sign of QSE in transport at least in the form of the quantum cut-off.

In summary, we analyzed quasi-classical interference between bulk and surface scattering processes in electron transport in thin films. The results acquire a very simple analytical form for high-quality films with large bulk mean free paths $\mathcal{L}_b$ and large lateral size of surface inhomogeneities $R$. There is a marked cross-over between two different interference regimes when $\mathcal{L}_b \sim R^2/a$. This crossover should manifest itself in change in the temperature dependence of the interference contribution when the electron-phonon scattering is the main bulk scattering channel or in change in the dependence on impurity concentration.

### 1.2.11 The quantum interference in a thin film

Resistivity of very thin metal films is an entangled combination of various surface and bulk scattering processes. The situation is further complicated because of the classical and quantum interference between different scattering channels. In this chapter, we try to understand the relative role that the interference between the surface and bulk scattering plays in the resistivity of ultrathin conductors in quantum size effect (QSE) conditions with noticeable quantization of electron motion. For QSE to be fully developed, it is necessary to go beyond the classical size effect which simply requires the bulk mean free path to be comparable to the film thickness. Below we assume that the resistivity of the bulk material is known and is described by the simplest bulk collision operator. For surface contributions, we will concentrate mostly on scattering by surface roughness assuming that the surface-driven reconstruction of the energy spectrum is less important as it is often the case in good metals. We will also neglect the scattering by grain boundaries; this is justified when the size of the boundaries is larger than both the bulk mean free path and the film thickness.

It is tempting to use the Mathiessen's approximation when the resistivity is due to two seemingly unrelated scattering channels such as bulk and wall scattering,

$$\rho^M = \rho_b + \rho_w, \tag{43}$$

and the same for the inverse transport times. Unfortunately, the real resistivity $\rho$ often differs significantly from the Mathiessen's value $\rho^M$, Eq. (43), due to various interference processes between the bulk and wall scattering channels. It is well known that the situation is even worse in the QSE conditions in which the use of the Mathiessen's equation (43) requires that both collision operators should have not just a diagonal, but the $\delta$-type structure with respect to quantized energy bands (we will encounter the clear signs of this below).

The entanglement between the surface and bulk contributions to conductivity comes from two mathematically distinct sources. First, there is what we would call for the lack of a better term, the "intrinsic interference" which describes the fact that the surface and bulk collision operators $\widehat{L}_w$ and $\widehat{L}_b$ are never strictly independent from each other. In diagrammatic language this corresponds to intersecting and overlapping of various bulk and surface interaction lines in the diagrammatic expansion for the Green's function. By rearranging the terms in the diagrammatic series, it is always possible to ascribe all the intrinsic interference contributions to either one of these two collision operators while keeping the other one "pure". In what follows, we assume that $\widehat{L}_b$ is the pure bulk collision operator, $\widehat{L}_b = \widehat{L}_b^{(0)}$ and that the interference terms are taken into account by the wall collision operator $\widehat{L}_w$, $\widehat{L}_w = \widehat{L}_w^{(0)} + \widehat{L}_{int}$.

However, even if these two operators were independent from each other (*i.e.,* the intrinsic entanglement could be neglected, $\widehat{L}_{b,w} \to \widehat{L}_{b,w}^{(0)}$), there is still the second source of interference which we will call the "mixing interference". Indeed, the source of this mixing can be easily understood if one considers, for example, the quantum transport equation with these supposedly independent $\widehat{L}_w^{(0)}$ and $\widehat{L}_b^{(0)}$,

$$\frac{dn}{dt} = \left(\widehat{L}_w + \widehat{L}_b\right) n. \tag{44}$$

The conductivity, which is proportional to the solution of this equation, would, therefore, contain the *inverse* operator $\left(\widehat{L}_w^{(0)} + \widehat{L}_b^{(0)}\right)^{-1}$. It is difficult to imagine the conditions, except for the simplest relaxation time approximation, under which this *inverse* operator can be decomposed into independent bulk and wall parts. This mixing, which is associated with inverting the overall collision operator, persists no matter whether we obtain the transport coefficients from solving the transport equation or from using the response function formalism such as, for example, the Kubo formulae. Note that in the relaxation time approximation corresponds to

a unique situation in which the operators $\widehat{L}_b$ and $\widehat{L}_w$ are completely independent *and* both have the $\delta$-type matrix structure.

To our best knowledge, earlier attempts to analyze the non-Mathiessen's behavior of resistivity did not pay attention to the existence of these two different sources of interference and dealt more often than not just with the mixing interference. More recent theoretical approaches still usually highlight just one of these two sources while neglecting the other. This often makes the comparison of the results rather meaningless. In those rare situations when the theoretical approaches are sufficiently general to cover the both sources, the results are somewhat convoluted and do not allow for easy interpretation and comparison with experiment. In this chapter, we trace both sources of interference simultaneously and analyze the conditions under which one of the interference mechanisms dominates over the other.

Below we will analyze both sources of interference in high quality ultrathin films in QSE conditions.

We are interested in conductivity of metal films in quasi-$2D$ films with random rough surfaces. QSE is caused by quantization of motion in the direction perpendicular to the film, $p_x \to \pi j\hbar/L$, where $L$ is the film thickness, and leads to a split of the energy spectrum $\epsilon(\mathbf{p})$ into a set of minibands, $\epsilon(p_x, \mathbf{q}) \to \epsilon(\pi j\hbar/L, \mathbf{q}) = \epsilon_j(\mathbf{q})$. One of the signature features of QSE in metals is a pronounced saw-tooth dependence of the lateral conductivity on, for example, film thickness, $\sigma(L)$, which is common for both bulk [37] and surface [8] scattering. However, in order to see this saw-tooth dependence in experiment with metal films, one has to overcome a difficulty which one does not encounter in semiconductors. The period of the saw-tooth QSE oscillations in the dependence $\sigma(L)$ is usually small, almost atomic, $\hbar/p_F$. For this reason, typical experimental objects are lead or semimetal films

such as bismuth. In most of other metal films the experimental curves are usually smooth. This means that for comparison with experiment our theoretical saw-tooth singularities should be averaged out and smoothed. This is not a major issue since the amplitude of the saw teeth is usually quite small. Recently we also predicted [20, 21] a new type of QSE with smooth curves $\sigma(L)$ and large-period oscillations of $\sigma(L)$ at relatively large values of $p_F L/\hbar$ that could lead to observation of QSE in a wider group of metals.

As mentioned earlier, the usual approach to transport in films is to account for bulk scattering processes via a collision operator in a transport equation and to relegate all boundary scattering to some boundary condition (for one of the best-known examples of earlier work of this type see Refs. [2]). If going this route, one should express the phenomenological parameters in the boundary condition (such as, for example, the specularity coefficient $p$ or the Namba [6] ratio of the amplitude of roughness and the mean free path, $\ell/\mathcal{L}_b$) via physical characteristics of surface. More sophisticated approaches with integro-differential boundary conditions could require even more parameters *in addition* to the geometrical and statistical properties of surface roughness. There are two issues associated with such approaches. First, one has to postulate the form of the boundary condition. This choice of the *form* of the boundary condition by itself imposes limitations, which are not always clear, on what kind of surface physics can or cannot be properly incorporated by this condition. More rigorous approaches of this type require the derivation of the boundary condition. When addressing the interference between bulk and boundary scattering, this derivation and, therefore, the resulting boundary condition should explicitly include the bulk scattering operator. As far as we know, no one has performed such a derivation.

Below we apply the results of our quantum diagrammatic transport derivation

[16] to the analysis of non-Mathiessen's terms. We will try to cut through the parameter clatter and get results that can be used for experimental applications. We will also try to look separately at the various sources of the interference and evaluate their relative importance. Where possible, we will simplify the results in the limit of ultraclean systems with large mean free path for which it is often possible to present the results as an expansion in inverse collision frequency.

### 1.2.12 Main equations in the quantum case

An important feature of ultrathin films is the quantization of motion across the film, $p_{xj} = \pi j\hbar/L$, which is responsible for quantum size effect (QSE) in transport and leads to a split of the $3D$ spectrum $\epsilon(\mathbf{p})$ into a set of $S$ minibands $\epsilon_j(\mathbf{q})$,

$$S = \mathrm{Int}\left[L/\pi a\right], \tag{45}$$

where the atomic-size constant $a = \hbar/p_F$ and $\mathbf{q}$ is the component of momentum along the film [in the simplest case of parabolic spectrum with the effective mass $m$, $\epsilon(\mathbf{p}) = p^2/2m$, the minibands are also parabolic, $\epsilon_j(\mathbf{q}) = (1/2m)\left[(\pi j\hbar/L)^2 + q^2\right]$]. As a result of this quantization, all the equations acquire the matrix character in the miniband index $j$.

After usual manipulations and expansion in harmonics, the quantum transport equation on the Fermi surface reduces to a set of linear equations

$$\frac{q_j}{m} = -\sum_{j'} \gamma_{jj'}\nu_{j'}\ , \tag{46}$$

where $q_j$ is the Fermi momentum in the miniband $j$, $q_j^2 = p_F^2 - (\pi j\hbar/L)^2$, $\nu_j$ describes the first angular harmonic (with respect to electric field $\mathbf{E}$) of the deviation of the distribution function from the equilibrium $\delta f^{(1)}$,

$$\delta f^{(1)}(q_j) = \nu_j\ \delta(\epsilon - \epsilon_F)\, eE, \tag{47}$$

and the matrix $\widehat{\gamma}$ is determined by the zeroth and first harmonics of the collision vertex,

$$\gamma_{jj'} = \delta_{jj'} \sum_{j''=1}^{S} \Gamma^{(0)}\left(q_j, q_{j''}\right) - \Gamma^{(1)}\left(q_j, q_{j'}\right). \tag{48}$$

In these notations, the conductivity and the transport time are

$$\sigma = -\frac{e^2}{3\hbar^2} \sum_j \nu_j\left(q_j\right) q_j \tag{49}$$

and

$$\tau_{tr} = \overrightarrow{q}\widehat{\gamma}^{\,-1}\overrightarrow{q} / \overrightarrow{q} \cdot \overrightarrow{q} \tag{50}$$

where the "vector" $\overrightarrow{q}$ is the set of parameters $q_j$. Note that $\sigma$ in Eq. (49) is already integrated across the film and is the $2D$ conductivity. It has the dimensionality of conductance and describes the density of current per unit area of the film.

In this chapter we are not interested in details of the bulk collision operator which has been thoroughly studied in the literature on metals. Therefore, for the bulk-related part of the matrices $\Gamma_{jj'}$ we will use the simplest possible expression by introducing the single bulk transport time $\tau_{tr}^b$,

$$\delta_{jj'} \sum_{j''=1}^{S} \Gamma_{jj''}^{b(0)} - \Gamma_{jj''}^{b(1)} = \frac{\delta_{jj'}}{\tau_{tr}^b}. \tag{51}$$

In contrast to the bulk scattering, for wall scattering we will use a more accurate description. In the end, the overall collision operator $\widehat{\gamma}$ in the transport equation (46) acquires the form

$$\begin{aligned} \gamma_{jj'} \;=\; & \frac{\delta_{jj'}}{\tau_{tr}^b} + \frac{\delta_{jj'}}{\tau_b} \sum_{j''=1}^{S} \int \frac{dq''q''}{4\pi} \frac{W_{jj''}^{(0)}\left(q_j, \overrightarrow{q}''\right)}{\left(\epsilon_{j''}(q'') - T_F\right)^2 + \hbar^2/4\tau_b^2} \\ & - \frac{1}{\tau_b} \int \frac{dq'q'}{4\pi} \frac{W_{jj'}^{(1)}\left(q_j, \overrightarrow{q}'\right)}{\left(\epsilon_{j'}(q') - T_F\right)^2 + \hbar^2/4\tau_b^2}. \end{aligned} \tag{52}$$

The poles in the surface scattering (integral) terms in Eq. (1), which are associated with bulk scattering $\mathrm{i}/\tau_{b'}$, are responsible for what we called the "intrinsic interference" in Introduction. The "mixing interference" appears because of the

need to invert the full operator $\widehat{\gamma}$ even though the bulk term $1/\tau_{tr}^{b}$ in the expression for the collision operator (52) has the simplest $\delta$-type form. Even if the roughness driven scattering probabilities $W_{jj'}$, Eq. (1), were diagonal in the miniband index $j$, there would have still been some mixing interference. The mixing interference disappears completely only if $W_{jj'} \propto \delta_{jj'}$.

Note that the bulk parameters $\tau_{tr}^{b}$ and $\tau_b$ in Eq. (52) could be significantly different: one represents the bulk transport time (the pole in the two-particle propagator) and the other - the collision time (the pole in the single-particle Green's function). Below I introduce parameter $\alpha$ for the ratio of these two times,

$$\frac{1}{\tau_{tr}^{b}} = \frac{\alpha}{\tau_b}. \tag{53}$$

If the bulk scattering is associated mostly with impurities, then $\alpha$ is a number of the order of 1. If, however, the main bulk collision channel is the electron-phonon scattering, then parameter $\alpha$ is small when the temperature is noticeably below the Debye temperature $T_D$,

$$\alpha \propto \left(T/T_D\right)^2 \ll 1. \tag{54}$$

Earlier [38], instead of inverting the collision operator (46), (52), I approximated the effect of collision operator by introducing the effective quasiclassical transport time as

$$\frac{1}{\tau_{tr}(\mathbf{p})} = \frac{1}{\tau_{tr}^{b}} + \frac{1}{\tau_b}\int \frac{W\left(\mathbf{p},\mathbf{p}'\right)\left(1-\cos\gamma\right)}{\left(\epsilon\left(\mathbf{p}'\right)-\mu\right)^2/\hbar^2 + 1/4\tau_b^2}\frac{d\mathbf{p}'}{\left(2\pi\hbar\right)^3} \tag{55}$$

with

$$\sigma = \frac{e^2\tau_{tr}}{m^2}\int \sum_{j'=1}^{S} \delta\left(\epsilon_j - \epsilon_F\right)\ q_j^2 \frac{qdq}{4\pi\hbar^2} = \frac{e^2 n \tau_{tr}^{(eff)}}{m},$$

where $W\left(\mathbf{p},\mathbf{p}'\right)$ is the quasiclassical surface scattering probability, *i.e.*, $W_{jj'}\left(\mathbf{q},\mathbf{q}'\right)$ with $j, j'$ replaced by $j^{(\prime)} = Lp_{x^{(\prime)}}/\pi\hbar$. As a result, I avoided the mixing interference

and concentrated on non-Mathiessen's interference terms $1/\tau_{tr}^{(int)}$ which are due to the difference of the integrand from the $\delta-$function,

$$\frac{1}{\tau_{tr}^{(int)}(\mathbf{p})} = \frac{1}{\tau_{tr}(\mathbf{p})} - \frac{1}{\tau_{tr}^{b}} - \int \delta\left(\epsilon_{j'}\left(q'\right) - T_F\right) W\left(\mathbf{p}, \mathbf{p}'\right)\left(1 - \cos\gamma\right) \frac{d\mathbf{p}'}{\left(2\pi\hbar\right)^2}, \quad (56)$$

and, therefore, describe what I called here the "intrinsic" interference. Note that such intrinsic interference has also been investigated in various contexts in Refs. [28–30] as well.

### 1.2.13 The quantum results

Below I will take QSE into account and perform an accurate inversion of the collision operator. One of the main feature of QSE is the saw tooth dependence of the conductivity of films on film thickness $\sigma\left(L\right)$ which, in principle, should be observed for both bulk [25] and surface [8] scattering. The reason is that the number of minibands $S$ increases by one each time the film thickness increases by $\delta L = \pi\hbar/p_F$. The change in $S$, by itself, should lead just to kinks on the curve $\sigma\left(L\right)$; what leads to a sharp drop in $\sigma$, and, therefore, to the saw tooth picture is the opening of a large number $S$ of new scattering channels each time $S$ changes by one. This means that the saw tooth dependence exists only as long as there are robust interband transitions which require the presence of noticeable off-diagonal elements in the matrix $\widehat{\gamma}$, Eq. (52). Since in this chapter the bulk part of the collision operator is approximated by a diagonal matrix, the saw tooth structure of the conductivity curve originates from the surface part of the collision operator.

I will analyze the relative contributions of intrinsic and mixing interference terms. Note that the mixing interference requires the non-$\delta$-type structure of the collision operator and is, therefore, associated with the saw tooth picture of QSE in conductivity of ultrathin films. In principle, the inversion of the collision operator (46) , (52), is a straightforward numerical task especially because I am interested in

thin films for which the number of minibands and, therefore, the rank of the matrix $\widehat{\gamma}$ are relatively low. The real difficulty here is not solving the quantum transport equation numerically, but making sense of the results because of a large number of different parameters, for many of which the experimental information is rather sparse. Thus one of the main goals is to cut through the parameter clatter and get physically meaningful results. Let us start from the list of relevant dimensionless parameters.

The interplay between bulk and roughness scattering can be described by two dimensionless parameters, $t$ and $u$, the first of which characterizes the bulk scattering and the second - the correlation of surface roughness:

$$t = \tau_b \; p_F^2/m \; \hbar, \;\; u = p_F^2 R^2/\hbar^2 \equiv R^2/a^2 \geq 1, \tag{57}$$

where $p_F$ is the Fermi momentum, and $a$, defined as $a = \hbar/p_F$, is of the order of the atomic size. It is often convenient to describe transport in films with large bulk mean free paths as an expansion in $1/t$. On the other hand, parameter $u$ accounts for the effectiveness of surface scattering in which the relative change in momentum is $\delta q/q \sim 1/\sqrt{u}$. The high-quality samples are the ones in which both $t$ and $u$ are large.

Apart from $t$ and $u$, other important dimensionless parameters include $\alpha$, which characterizes the difference between the bulk collision and transport times (53), the dimensionless thickness of the film $L/a$, and the amplitude of roughness $\ell/a$. In these notations, the bulk mean free path $\mathcal{L}_b$ is

$$\mathcal{L}_b/a = \tau_{tr}^b v_F/a = t/\alpha. \tag{58}$$

With so many parameters, none of which reduces to a simple scaling, one should find a way to understand the hierarchy of competing effects that would allow one to get some clarity.

Nevertheless, one of the parameters - $\alpha$ or $\ell/a$ - can still be excluded by a proper choice of variables leaving behind only the ratio

$$\theta = \frac{\alpha a^2}{\ell^2}. \tag{59}$$

To achieve this, I will describe the relative interference contribution to the resistivity $\rho$ and transport time $\tau_{tr}$ by parameter $\chi$,

$$\chi = \frac{\rho - \rho^M}{\rho^M} \equiv \tau_{tr}^M \left( \frac{1}{\tau_{tr}} - \frac{1}{\tau_{tr}^M} \right), \tag{60}$$

where the Mathiessen's resistivity $\rho^M$ and transport time $\tau_{tr}^M$ are defined by the following equations

$$\rho^M = \rho_b + \rho_w, \; 1/\tau_{tr}^M = 1/\tau_{tr}^b + 1/\tau_{tr}^w, \tag{61}$$

and indices $b$ and $w$ refer to the pure independent bulk and wall contributions.

The collision operator $\gamma_{jj'}$, Eq. (52), contains two terms. The bulk one is proportional to $\alpha$ and the wall one - to $\ell^2/a^2$. If instead of $\gamma_{jj'}$ I will introduce the matrix

$$\widetilde{\gamma}_{jj'} = \frac{a^2}{\ell^2} \gamma_{jj'}, \tag{62}$$

this matrix will depend on $\alpha$ and $\ell^2/a^2$ only in the combination $\theta$, Eq. (59). This means that the solution $\widetilde{\nu}_j = (\ell^2/a^2)\, \nu_j$ of the renormalized equation (59) will also depend only on $\theta$. The same will be true for the renormalized conductivity, $\widetilde{\sigma} = \sigma\,(\ell^2/a^2)$, resistivity $\widetilde{\rho} = \rho\,(a^2/\ell^2)$, and the inverse transport time, $1/\widetilde{\tau}_{tr} = (a^2/\ell^2)\,/\tau_{tr}$. Then the relative interference contribution (60),

$$\chi = \frac{\rho - \rho^M}{\rho^M} \equiv \left( \frac{1}{\widetilde{\tau}_{tr}} - \frac{\theta}{\tau_b} - \frac{1}{\widetilde{\tau}_{tr}^w} \right) / \left( \frac{\theta}{\tau_b} + \frac{1}{\widetilde{\tau}_{tr}^w} \right), \tag{63}$$

will also contain $\alpha$ and $\ell$ only in the form of the combination $\theta$. The pure roughness-driven transport time $\widetilde{\tau}_{tr}^w$ in Eq. (63) should be calculated using the surface scattering probabilities $W_{jj'}$, Eqs. (2)\,, (3), without the factor $\ell^2/a^2$(and, of course, in the limit $\tau_b \to \infty$).

Note, that parameter $\theta/t$ provides one with an estimate for comparative contributions of surface and bulk scattering channels to transport, $\tau_{tr}^{w}$ and $\tau_{tr}^{b}$. However, this estimate is not very accurate because of a strong dependence of $\tau_{tr}^{w}$ on $L/a$ and $u$, Eq. (4). The ratio $\tau_{tr}^{b}/\tau_{tr}^{w}$ is best characterized by the scaled function $\phi\left(L/a,u\right)$,

$$\frac{\tau_{tr}^{b}}{\tau_{tr}^{w}}=\frac{t}{\theta}\phi\left(L/a,u\right), \tag{64}$$

which depends only on $u$ and $L/a$. The function $\phi\left(L/a\right)$,

$$\phi=\frac{\mathbf{q}\cdot\mathbf{q}}{\mathbf{q}\cdot\widehat{F}^{-1}\mathbf{q}}, \tag{65}$$

where,

$$F_{jj'}=4\pi^{5}\left(\frac{L}{a}\right)^{6}j^{2}\;u\;e^{-u}\exp\left(c_{j}/2\right)f_{jj'}, \tag{66}$$

and,

$$\begin{aligned} f_{jj'} &= \delta_{jj'}\sum_{j''}\left(j''^{2}\exp\left(c_{j''}/2\right)I_{0}\left(u\sqrt{1-c_{j}/u}\sqrt{1-c_{j''}/u}\right)\right) \\ &\quad -j'^{2}\exp\left(c_{j'}/2\right)I_{1}\left(u\sqrt{1-c_{j}/u}\sqrt{1-c_{j'}/u}\right), \end{aligned} \tag{67}$$

with,

$$c_{j}\;=\pi^{2}\;u\left(\tfrac{a}{L}\right)^{2}j^{2}, \tag{68}$$

is presented in Figure 4 for several values of $u=p_{F}^{2}R^{2}/\hbar^{2}$.

Note that the thickness of the film, $L/a$, enters the expression for $\phi$, Eq. (65), not only as explicit coefficients but also through the upper limit of summation over $j,j',j''$ since the total number of accessible minibands

$$S=\mathrm{Int}\left[L/\pi a\right]. \tag{69}$$

It is clear that even the pure wall contribution is comparable to the bulk term at not very small $\alpha$ only for relatively thin films. This means that the interference

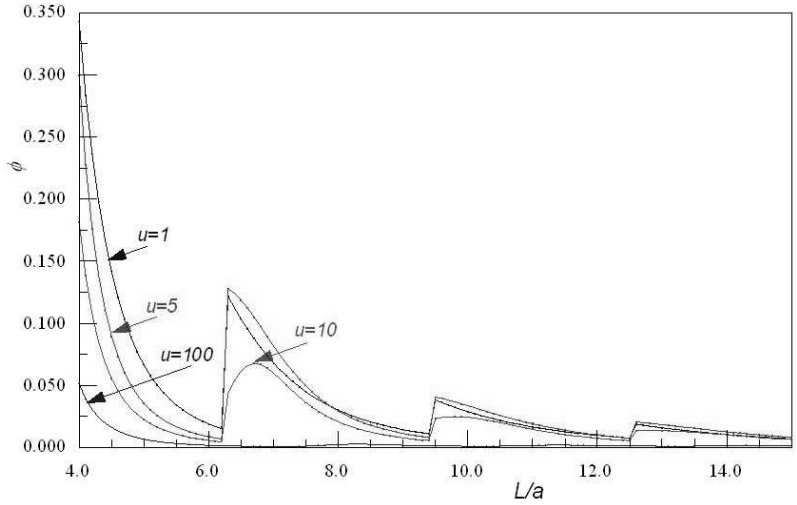


Figure 4. The function $\phi\,(L/a)$, for different $u$.

terms, which are small in comparison with both pure surface and bulk contributions, should be investigated for relatively thin films for which the pure surface contribution is not negligible in comparison with the bulk one, *i.e.*, the function $\phi\,(L/a, u)$ is not exceedingly small.

Figure 4 confirms that the surface contribution decreases with increasing $u$ since the film surface becomes more and more smooth. The second observation is that the increase in $u$, *i.e., in* $R/a$, results in smoothing of the saw teeth at $L/a = \pi j$, which correspond to usual QSE, and leads eventually to the appearance of a new type of QSE in accordance with Ref. [20, 21].

As it was indicated above, one of the main issues when dealing with the interference between the bulk and surface scattering is to separate the sources of intrinsic and mixing interference. I continue this section with analysis of the pure intrinsic interference. This is a reasonable approximation for pure films at low temperatures for which $\alpha \ll 1$, Eq. (54). After that, I will analyze the pure mixing interference by assuming $\tau_b \to \infty$ in the *integral* term only in Eq. (52).

As we will see, this approximation might work reasonably well for films with the dominant impurity scattering in the bulk. Towards the end of the section, I will look at general results with both types of interference and will try to compare their contribution under various conditions.

### 1.2.14 The intrinsic interference

In this subsection I will consider the pure intrinsic interference. There are two different sets of conditions under which the mixing interference becomes negligible. The first one is, of course, the case of the vanishingly small value of $\alpha$. This situation occurs in ultraclean films at low temperatures when the bulk scattering is dominated by the longwave phonons making the ratio of bulk collision and transport times $\alpha$ very small, Eq. (54). In this case one can simply put $\alpha = 0$ in the collision operator Eq. (52), (53). Since in this case the bulk transport time and conductivity are negligible by design, the relative intrinsic interference contribution (60) reduces to

$$\chi_{intr} = \frac{\rho(\alpha = 0) - \rho_w}{\rho_w} \equiv \tau_{tr}^w \left( \frac{1}{\tau_{tr}(\alpha = 0)} - \frac{1}{\tau_{tr}^w} \right), \tag{70}$$

where, as above, $\rho_w$ and $\tau_{tr}^w$ are the pure wall-driven resistivity and transport time in the absence of bulk scattering (*i.e.*, the resistivity and transport time generated by the collision operator (52) with $\alpha = 0$ and $\tau_b \longrightarrow \infty$). Since here I assume from the start that $\alpha = 0$, there is no need to replace the transport times $\tau$ in the right hand side of Eq. (70) by their renormalized values as in Eq. (63) - the parameter $\ell^2/a^2$ will get cancelled automatically.

In this case, the only remaining parameters in $\chi_{intr}$ are $t, u$, and $L/a$. In high-quality films, parameter $t$ (*i.e.*, $\tau_b$) is large, and it is often convenient to expand the integrand in Eq. (52) in $1/t$ using

$$\frac{1/x\pi}{\left(\epsilon(\mathbf{p}') - T_F\right)^2 + 1/x^2} = \delta\left(\epsilon_{j'}(q') - T_F\right) + \frac{1}{x}\frac{d\delta\left(\epsilon_{j'}(q') - T_F\right)}{d\epsilon} \tag{71}$$

$$+\frac{1}{2x^2}\frac{d^2\delta\left(\epsilon_{j'}\left(q'\right)-T_F\right)}{d\epsilon^2}+... \tag{72}$$

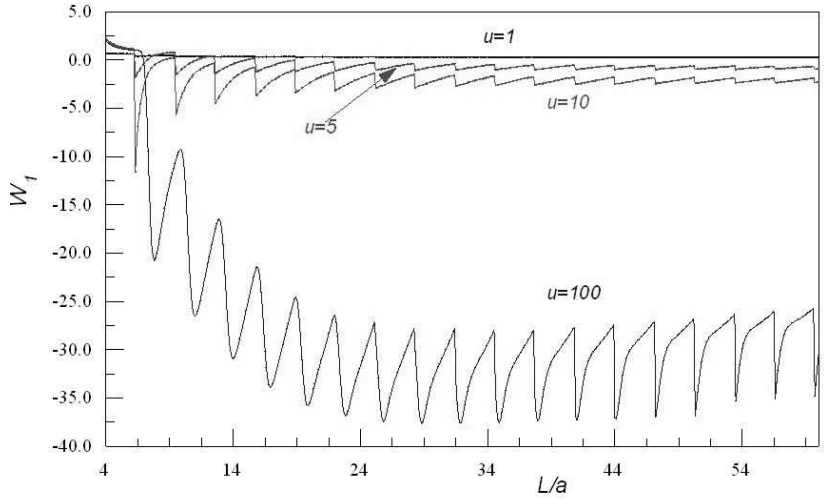


Figure 5. The coefficient $W_1$ for different $u$.

The first, $\delta-$function term in this expansion in the collision operator eventually generates the pure wall-driven resistivity and transport time $\rho_w$ and $\tau_{tr}^w$. Then the relative interference contribution $\chi_{intr}$ becomes

$$\chi_{intr}=\frac{1}{t}W_1\left(u,L/a\right)+\frac{1}{t^2}W_2\left(u,L/a\right)+... \tag{73}$$

The plots of functions $W_{1,2}\left(L/a\right)$ for several values of $u$ are given in Figs. 5, 6. The figures indicate that the relative interference contributions to the resistivity are almost always negative in the case of pure intrinsic interference except for extremely thin films. Another observation is that the intrinsic interference at large $u$ looses the saw tooth structure of the usual QSE and acquires the QSE of Ref. [20, 21].

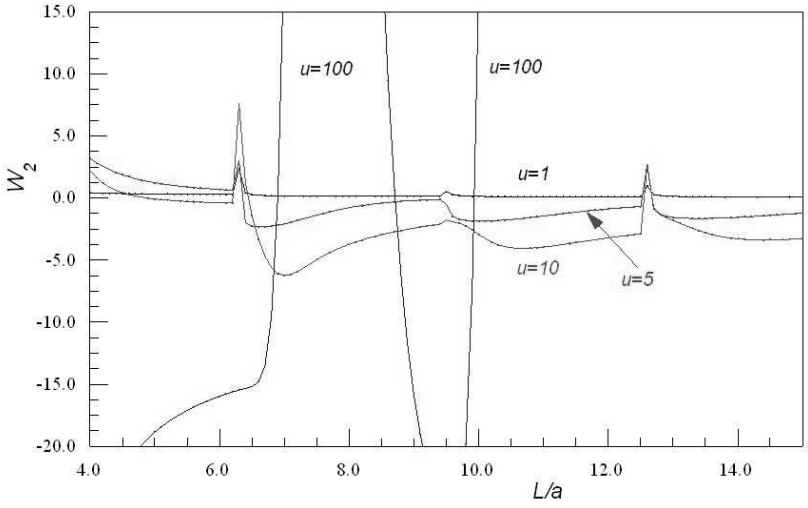


Figure 6. The coefficient $W_2$ for different $u$.

A more important observation concens slightly thicker films than the ones in Figs. 5 and 6. With further increase in thickness, the values of coefficients $W_1$ for all values of $u$ and $W_2$ for smaller $u$ remain more or less the same while $W_2$ $(u = 100)$ rapidly increases by an order of magnitude, Fig. 6a. This means that in high quality films with large values of $t$ and $u$ the intrinsic interference can experience a crossover from $1/t$ to $1/t^2$ behavior at large enough values of $u$. earlier I observed a similar crossover in our quasiclassical description of the intrinsic interference in Ref. [38]. Fig. 6a also shows, in accordance with Ref. [20, 21], a restoration of the usual saw tooth QSE for thicker films for which $L/a \gg R/a = \sqrt{u}$.

The second situation with the dominant intrinsic interference is, with certain caveats, the case of a diagonal matrix $\widehat{\gamma}$, Eq. (52), *i.e.,* the diagonal matrix of roughness-driven scattering probabilities $W_{jj'}$, Eqs. (2) , (3). This can happen for large scale roughness, $u = R^2/a^2 \gg L^2/a^2$ when the scattering-driven change in

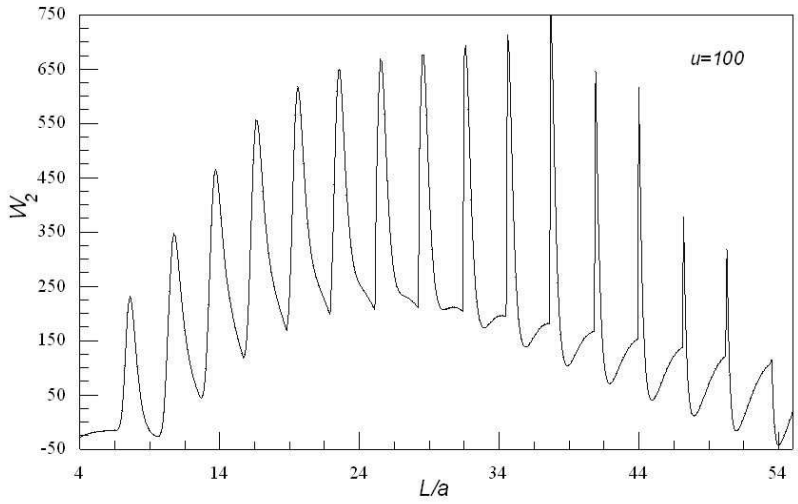


Figure 7. The coefficient $W_2$ at $u = 100$ for thicker films.

the particle momentum $\delta q \sim \hbar/R$ is insufficient for the particle transition between the minibands, $\delta q/q \sim 1/\sqrt{u} \ll 1$. When the collision operator $\widehat{\gamma}$ is diagonal,

$$\gamma_{jj'} = \gamma_j \delta'_{jj'},$$

the solution of the transport equation (46) is trivial,

$$\frac{q_j}{m} = -\sum_{j'} \gamma_{jj'} \nu_{j'} \ , \nu_j = -q_j \gamma_j^{-1}/m \tag{74}$$

and the full transport time $\tau_{tr}$, Eq. (50), is quite simple:

$$1/\tau_{tr} = \sum q_j^2 / \sum q_j^2 \gamma_j^{-1}. \tag{75}$$

Since the wall contributions to $\gamma_j$ are different while the bulk ones are the same, $\alpha/\tau_b$, Eq. (75) still contains noticeable mixing terms. However, the structure of the roughness-driven scattering probabilities $W_{jj'}\left(\mathbf{q}_j - \mathbf{q}'_{j'}\right)$, Eqs. (2) , (3) , is such that the diagonal terms $W_{jj}$ differ from each other only by the factors $j^4$. Since $q_j^2$ decrease with increasing $j$, the overall transport time $1/\tau_{tr}$, Eq. (75), can with good accuracy be rewritten as

$$1/\tau_{tr} \approx \frac{\gamma_1}{q_1^2} \sum q_j^2 = \frac{1}{q_1^2} \left( \frac{\alpha}{\tau_b} + \frac{1}{\tau_{11}^w} \right) \sum q_j^2, \tag{76}$$

where $1/\tau_{11}^{w}$ is the integral term with $W_{11}$ in the expression for $\gamma_{jj'}$, Eq. (52). The approximation (76) emphasizes the dominant role of gliding particles in the lateral transport in quantized ultrathin films. This equation contains only the intrinsic interference. The plot of the corresponding function $\chi$ is given in Figs. 10-12.

### 1.2.15 The mixing interference

The mixing interference can be obtained by formally putting $\tau_b \longrightarrow \infty$ in the wall-driven part of the collision operator (52). Then the bulk relaxation time enters $\chi_{mix}$, Eqs. (60), (63) , only in the combination $\theta/t$,

$$\chi_{mix} = \chi_{mix}\left(\theta/t, u, L/a\right). \tag{77}$$

Unfortunately, the structure of $\chi_{mix}$ is such that all its variables - $\theta/t, u, L/a$ - enter the equations independently and none of the variables reduces to simple scaling of $\chi_{mix}$ or can be eliminated.

One should be very cautious when inverting the collision operator numerically. The roughness-driven part of the collision operator (52) was calculated in Ref. [16] only to the main order in the roughness amplitude $\ell$. Therefore, many higher order terms in $\ell^2$, which arise from the inversion of the collision operator, should be disregarded.

To solve the transport equation and, therefore, calculate the transport time, one should simply invert the collision operator (matrix) $\widetilde{\gamma}_{jj'}$. The wall-driven part of the matrix $\widetilde{\gamma}_{jj'}$, Eq. (52), in the limit $\tau_b \longrightarrow \infty$ corresponds to the first, $\delta$-type term in expansion (71) and becomes relatively simple. Using the notations of Ref. [20, 21], the matrix $\widetilde{\gamma}_{jj'}$ can then be rewritten as

$$\begin{aligned} \widetilde{\gamma}_{jj'} &= \frac{a^2}{\ell^2}\gamma_{jj'},\ \gamma_{jj'} = \frac{\alpha\delta_{jj'}}{\tau_b} + \frac{1}{\tau_{jj'}},\ q_j/m = -\sum_{j'}\nu_{j'}\left(q_{j'}\right)/\tau_{jj'}, \qquad (78) \\ \frac{1}{\tau_{jj'}} &= \frac{m}{2}\sum_{j''}\left[\delta_{jj'}\,W_{jj''}^{(0)} - \delta_{j'j''}\,W_{jj'}^{(1)}\right]. \end{aligned}$$

In the case of the Gaussian correlation functions, the harmonics of the scattering probabilities $W$ are given as

$$\zeta^{(0)}\left(q_j, q_{j'}\right) = 4\pi\ell^2 R^2 \left[e^{-QQ'} I_0\left(QQ'\right)\right] e^{-(Q-Q')^2/2}, \quad (79)$$

$$\zeta^{(1)}\left(q_j, q_{j'}\right) = 4\pi\ell^2 R^2 \left[e^{-QQ'} I_1\left(QQ'\right)\right] e^{-(Q-Q')^2/2}, \quad (80)$$

$$W_{jj'}^{(0,1)}\left(\mathbf{q}, \mathbf{q}'\right) = \frac{\hbar}{m^2 L^2}\left(\frac{\pi j}{L}\right)^2 \left(\frac{\pi j'}{L}\right)^2 \zeta^{(0,1)}. \quad (81)$$

where where $Q = q_j R$, $Q' = q_{j'} R$ (the corresponding equations for some other classes of the correlation functions can be found in Ref. [20, 21]).

Since $\theta$ and $t$ enter the matrix $\widetilde{\gamma}_{jj'}$,Eq. (78), only in the combination $\theta/t$ and only directly via the diagonal elements, the inversion of this matrix obviously makes $\chi_{mix}\left(\theta/t\right)$ a rational function of the polynomials of $\theta/t$. Since $\chi_{mix}\left(\theta/t = 0\right) = 0$, such structure of $\chi_{mix}\left(\theta/t\right)$ means that at $\theta/t \ll 1$

$$\chi_{mix}\left(\theta/t \ll 1\right) = \frac{\theta}{t} V_1\left(u, L/a\right) + \frac{\theta^2}{t^2} V_2\left(u, L/a\right) + ... \quad (82)$$

These functions are illustrated in Figs. 7,8. Note that since $\theta$ contains a small parameter $\ell^2$ in denominator, the condition $\theta/t \ll 1$, necessary to justify expansion (82) is much stronger than a simple condition of large bulk free paths $t \gg 1$ necessary for expansion (73) unless one deals with ultraclean films at ultralow temperatures for which $\alpha \ll 1$.

The mixing interference contribution $\chi_{mix}$ outside of domain (82) is illustrated in Figs. 9,10. The existence of the mixing interference is related to the presence of the off-diagonal terms in the collision operator $\widehat{\gamma}$, Eq. (52). If this whole matrix were of $\delta$-type, as its bulk-driven counterpart is assumed to be in this chapter, the inversion would have been trivial and the intrinsic interference from the previous subsection would have been the only interference mechanism. The wall-driven scattering probability $\widehat{W}$, Eqs. (2) , (3), is indeed close to being diagonal at very

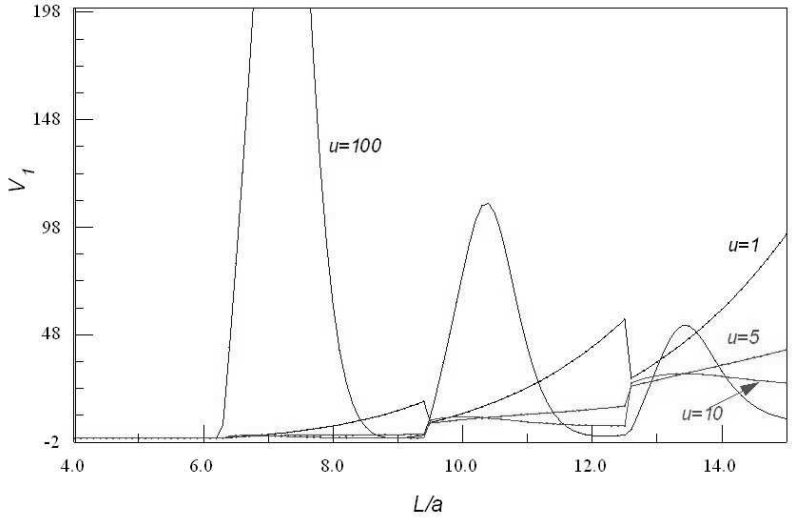


Figure 8. The coefficient $V_1$ for different $u$.

large values of the correlation radius $R$ (large $u$) when the scattering driven change in momentum $\delta q \sim \hbar/R$ is too small to ensure transitions between the minibands. Still, even in this case one can observe a spontaneous, and very sharp, opening of transition channels $j \longleftrightarrow j+1$ when the film thickness reaches some critical value $L_j = \sqrt{(j+1/2)\, aR/2}$, Ref. [20, 21]. It is instructive to analyze how this new type of quantum size effect not only results in a strong precipitous drop in conductivity [20, 21], but also leads to the reemergence of the mixing interference.

At large $R$, when the thickness of the film approaches the value of $L_1$, the previously diagonal matrix $\widehat{\gamma}$, Eq. (52), acquires the first off-diagonal element,

$$\gamma_{12} = \gamma_{21} = 1/\tau_{12}^{w}. \tag{83}$$

The value of $\tau_{12}$ decreases exponentially when $L$ approaches $L_1$ and becomes practically equal to the wall-driven part of the diagonal elements $\gamma_{11,22}$ which in this case are approximately $1/\tau_{tr}^{w}$. The overall transport time also rapidly drops with

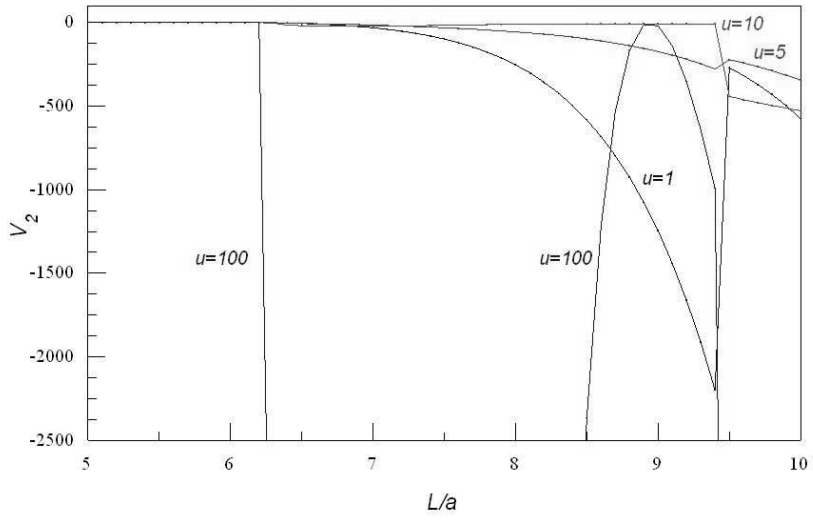


Figure 9. The coefficient $V_2$ for different $u$.

decrease in $\tau_{12}^w$ as

$$\frac{1}{\tau_{tr}} \sim \frac{\alpha}{\tau_b} + \frac{1}{\tau_{tr}^w} - \frac{1}{\tau_{12}^w} - \frac{1}{\tau_{12}^{w2}} \frac{\tau_b \tau_{tr}^w}{\alpha \tau_{tr}^w + \tau_b} = \frac{1}{\tau_{tr}^M} - \frac{1}{\tau_{12}^w} - \frac{\tau_{tr}^M}{\tau_{12}^{w2}} \tag{84}$$

meaning that the mixing interference grows by the absolute value starting from zero as

$$\chi_{mix} = -\frac{\tau_{tr}^M}{\tau_{12}^w} \left(1 + \frac{\tau_{tr}^M}{\tau_{12}^w}\right) \tag{85}$$

until it reaches approximately

$$\chi_{mix} \sim -\left(\frac{\alpha \tau_{tr}^w}{\tau_b} + 1\right)^{-2} \left(2 + \frac{\alpha \tau_{tr}^w}{\tau_b}\right) \tag{86}$$

$$= -\left(\frac{\theta}{t\phi} + 1\right)^{-2} \left(2 + \frac{\theta}{t\phi}\right) \tag{87}$$

at $\tau_{12}^w \sim \tau_{tr}^w$. Eq. (86) gives a good estimate of the mixing interference for walls with large-scale roughness $R \gg a$.

### 1.2.16 General results

The above analysis of intrinsic and mixing interference can serve as a guide for study of interference effects in more general situations. For example, Figure

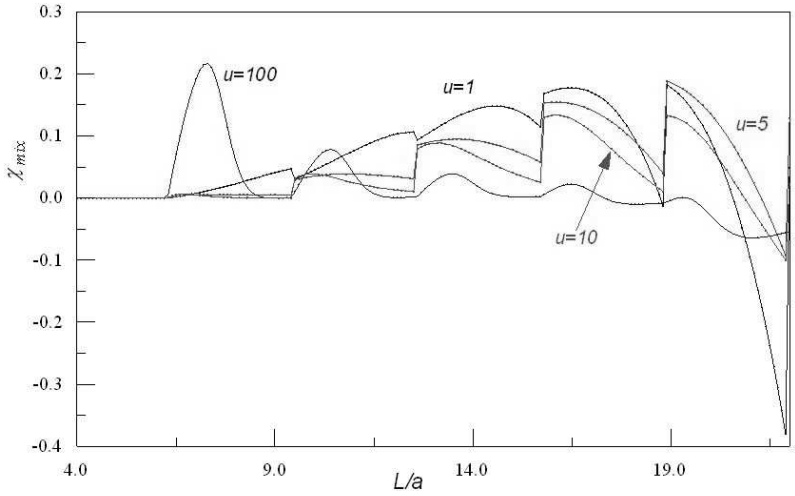


Figure 10. The mixing interference $\chi_{mix}$.

10 represents a dependence of the relative interference contribution $\chi$, Eq. (60), on film thickness at various values of $t$, $t = 1; 50; 100$, for films with small-scale roughness, $u = 1$ and $\theta = 0.1$. For comparison, I plotted in the same figure the relative mixing interference (dashed lines marked as $mix$), $\chi_{mix}(L/a)$, for the same values of parameters. The difference between the solid and dashed curves reflects the contribution from intrinsic interference. Since the mixing interference is suppressed for single-band systems, *i.e.,* at $L/a < 2\pi$, it is absolutely clear that the intrinsic interference dominates in ultrathin films and is gradually being replaced by the mixing interference with increasing thickness. Of course, since the value of $\theta$ here is not small, the mixing interference dominates in thick films. Interestingly, it looks like the intrinsic interference contribution is almost always negative while the mixing one is positive. The overall interference contribution tends to be destructive in very thin films and constructive in thicker ones.

Figure 10a extends the curves $\chi(L/a)$ and $\chi_{mix}(L/a)$ (also at $u = 1$ and $\theta = 0.1$) to thicker films. It is clear that the interference contribution exhibits a

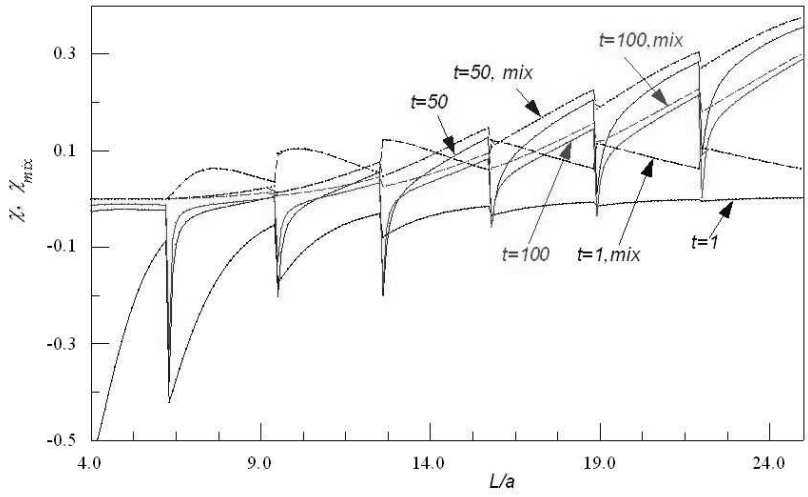


Figure 11. The full and mixing interference, $\chi$ and $\chi_{mix}$ at $u = 1$, $\theta = 0.1$.

maximum at certain thickness and that the positions of the maxima shift to the right with the increase in the bulk mean free path (with the increase in $t$). In very thick films, the bulk scattering obviously dominates the resistivity and all boundary processes, including the interference ones, become negligible meaning that $\chi\,(L/a \to \infty) \to 0$.

The dependence of $\chi$ and $\chi_{mix}$ (dashed lines marked with the letter $m$) on $\theta = \alpha/\ell^2$ is illustrated in Figure 11 at $t = 20$ and $u = 1$. Here again at $L/a < 2\pi$ I have a pure intrinsic interference, mostly destructive, which is gradually being replaced by the constructive mixing interference for thicker films. The replacement occurs faster at higher values of $\theta$. Interestingly, the saw tooth structure of the curves is much more pronounced for the overall and, therefore, intrinsic interference than for the mixing one. I do not have a simple explanation for this effect.

The small values of $\theta$ for the curves in Figure 11 should be interpreted as the consequences of small values of $\alpha$ rather than large values of $\ell/a$: the computations were done at $u = 1$ while our theory is valid at $\ell/a < \sqrt{u}$. If one wants to suppress

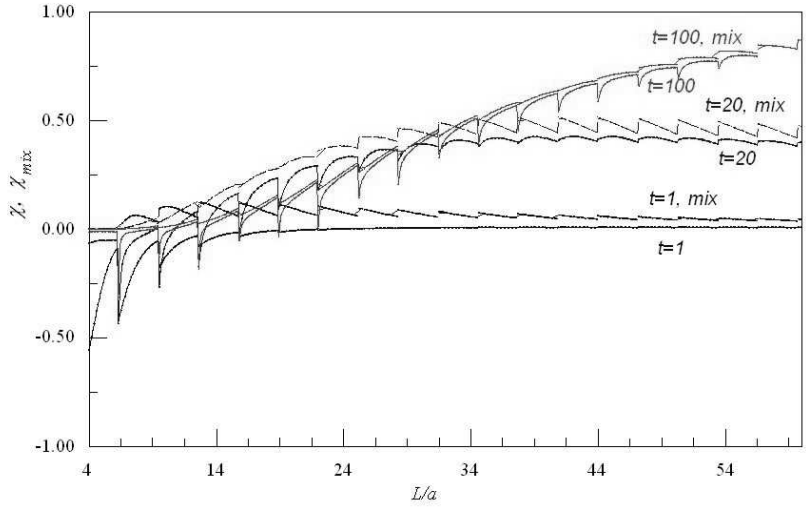


Figure 12. $\chi$ and $\chi_{mix}$ for thicker films.

$\theta$ by increasing the amplitude of inhomogeneities $\ell/a$, one should simultaneously increase the correlation radius of surface roughness $R/a \sim \sqrt{u}$.

Finally, Figure 12 presents the curves $\chi\,(L/a)$ (solid lines) and $\chi_{mix}\,(L/a)$ (dashed lines marked as $m$) for $t = 20$ and $\theta = 0.1$ at various values of $u$, $u = 1; 10; 100$. The curves at $u = 100$ differ from all the rest in that the contribution from intrinsic interference here seems to be positive. Also, the QSE of Ref. [20, 21] is much more pronounced for the intrinsic and overall interference than for the mixing interference. This is quite understandable since this type of QSE practically never shows up when the bulk collisions present the dominant scattering channel (see discussion in the second Ref. [20, 21]).

### 1.2.17 Summary of the quantum case

In summary, I analyzed interference between bulk and surface scattering processes in resistivity of thin films in quantum size effect (QSE) conditions. General results can sometimes be not very transparent because of parameter clatter. The main parameters that affect the interference are the pure bulk transport time, the

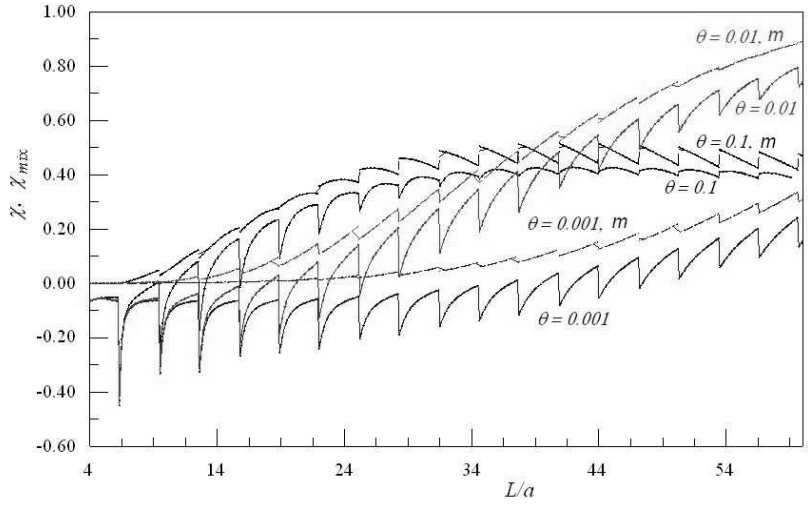


Figure 13. $\chi$ and $\chi_{mix}$ for different $\theta$.

amplitude and the correlation radius of surface roughness, the film thickness, and the ratio of the bulk transport and collision times. Such a rich parameter space can not only significantly affect the value of the interference contributions, but even change its sign.

The uncertainty in some of the parameters, especially the values of the bulk transport and collision times, makes comparison with experiment not very straightforward. On the other hand, there is currently one experimental group that measures the thin resistivity simultaneously with the STM analysis of the surface (see Refs. [14, 15, 19, 34] and references therein). To the best of our knowledge, none of the experimental group observed clear signs of QSE in resistivity which makes a direct comparison of our results with experimental data virtually impossible. One of the options here is to average out the QSE gyrations and compare averaged data to experiment. I tried to follow this route with respect to the dependence of the resistivity on film thickness. However, depending on the method of averaging of the same curve, the results for the transport time exhibited the functional

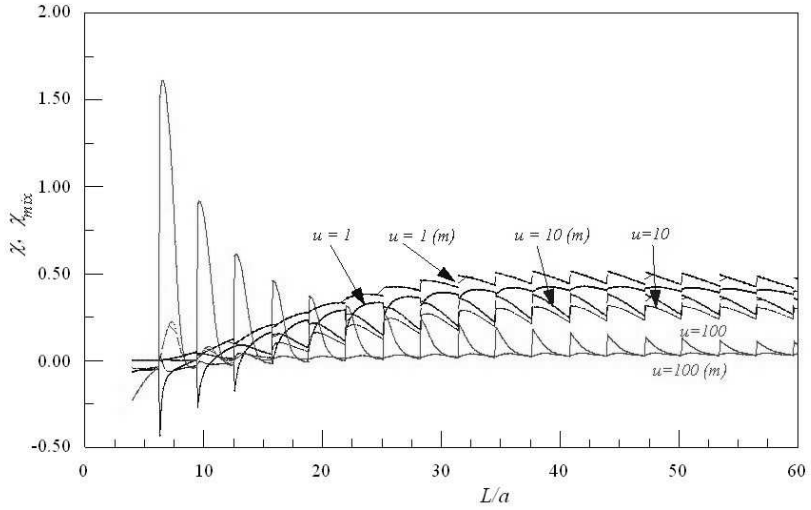


Figure 14. $\chi$ and $\chi_{mix}$ for different $u$

dependence anywhere between $L^{-2.3}$ when using the tops of the peaks and $L^{-0.6}$ when using the minima. Most of all experimental curves, which also exhibit a large uncertainty (see discussion in Ref. [38]), fit within this range.

Our main emphasis was on revealing and following two distinct sources of such interference - the entanglement between surface and bulk interaction lines in the self-energy of the single-particle Green's functions and the mixing resulting from the inversion of the collision operator in the generalized response function. I labeled these two types of interference in the chapter as "intrinsic" and "mixing" interference. The intrinsic and mixing interference lead to different types of behavior of non-Mathiessen's terms in resistivity of thin films. Earlier approaches included only the mixing interference (see Refs. [7, 13–15] and references therein) though some of recent publications concentrated on intrinsic interference, Refs. [28–30] without paying attention to the mixing one.

In generic situation, the mixing terms are larger than the intrinsic ones in thicker films. However, there are several important situations when the intrinsic

interference clearly dominates. First, this happens in ultrathin films. When the thickness of the film $L$ is such that the QSE reduces the spectrum to a single miniband, $L/a < 2\pi$, the mixing interference is completely suppressed and only gradually picks up with increasing thickness. Second, since the intrinsic interference is built of the bulk collision time $\tau_b$ while the mixing one contains the bulk transport time $\tau_{tr}^b$, the intrinsic interference can dominate when there is a considerable gap between these two times. This can happen, for example in pure films at low temperatures when the bulk relaxation is due mainly to the phonon scattering. In this case the bulk transport time can exceed the collision one by a large factor $(T_D/T)^2$ resulting in the dominant role of the intrinsic interference effects.

I tried to compare our results with other quantum computations which explicitly include QSE [7, 8, 13, 16]. Most of earlier publications did not pay sufficient attention to the interference effects. Refs. [7] do not contain any explicit equations for the interference terms that can be compared with our results. The authors of Ref. [8] were not interested in the interference terms and considered bulk and roughness scattering as two independent additive channels. Ref. [13] also does not contain any explicit information about the interference terms except for mentioning that these contributions seem to be smaller than the pure wall or bulk terms. As our results show, this is not always the case and the relative interference contribution $\chi$ can be quite large. In addition, Refs. [7, 8, 13] use the $\delta$-type (white noise) approximation for the surface roughness and, therefore, cannot describe the large-scale roughness and the corresponding crossover between different regimes.

In most of the parameter space the contribution from the intrinsic interference (thinner films) tends to be negative (destructive) and from the mixing one (thicker films) - positive (constructive). This qualitatively agrees with the experimental observation in Refs. [19, 34]. The quantitative comparison is currently impossible

since there are no yet confirmed observations of QSE in metals.

## 1.3 Interference in a trapped strongly interacting BEC

The study of the Bose condensation (BEC) of alkali gases in traps has became the focal point in atomic, low temperature, and condensed matter physics. Phenomena that have been discussed earlier only within theoretical models (see review [39]) can now be observed in these systems. The phenomena in ultracold alkali gases are incredibly rich and combine features inherent to diverse condensed matter and low temperature systems (Refs. [40] and references therein) from "classical" superfluid or superconducting systems [40] to spin-polarized quantum gases [41] to Mott transition in the optical lattice [42, 43].

The inhomogeneity of the trapping potential is an unavoidable feature of trapped BECs. The interplay between the repulsive interaction and the trapping potential complicates BEC. From early on, it was clear that the interaction and the trap have opposite effects on condensation [44, 45]: while the trap tends to concentrate the condensate in a narrow region of space around the particle ground state in the trap, the repulsion widens this condensate droplet. A combined analytical description has been elusive and our previous experience with condensation in homogeneous systems is not very helpful. The problem becomes even more complex in the presence of the optical lattice inside the trap which adds two different localization processes - Mott transition and localization of narrow band particles by an inhomogeneous potential.

I analyze a situation where it is possible to get an accurate semi-analytical picture of the condensation in trapped interacting gases. The main goal in this section is the comparison of the condensate formation in traps with and without an optical lattice inside. The main attention is paid to the index in the temperature dependence of the condensate fraction and to the size of the condensate droplet. It

turns out that this index is not universal even for a low density gas. Furthermore, the effective dimensionality of the problem depends on the presence of the optical lattice and changes with condensation making the later stages of BEC different from initial.

I begin with a more conventional and transparent problem of BEC in trapped gases in the absence of the optical lattice. Later, I add the complications associated with the optical lattice. A similar calculation without the optical lattice was performed in Ref. [46] though at a noticeably lower population of the trap. This difference strongly affects the results. I assume that the density is still sufficiently low to neglect the interaction before the onset of condensation even in the center of the trap. In computations, this condition limits the total number of particles in our trap $N$ to $N < 10^6$. This also means that the critical temperature $T_c$ for the onset of condensation is practically unaffected by the interaction. The interaction is brought into play only after the start of condensation, at $T < T_c$, since the particles condensate in the center of the trap making the density in the center large. Thus, the interaction, which is proportional to the particle density, is large only in and around the condensate droplet. The normal particles are pushed out by the dense condensate towards the periphery of the trap where the interaction is negligible. However, the further particles move away from the center the higher is the gradient of the trapping potential which is responsible for the force pushing the normal particles back towards the trap center. Therefore, at the *later* stages of BEC, the majority of remaining normal particles are distributed in an almost two-dimensional shell around the condensate droplet and the dimensionality of the condensation problem changes from the three-dimensional in the beginning of the condensation to quasi-$2D$ later on.

I consider a $3D$ harmonic trap with a single-particle ground state of frequency

$\omega$ and spacial size $\sigma_0$ (the axial asymmetry of experimental traps is largely irrelevant in our context). Without interaction, BEC starts at $T_c = 0.941\hbar\omega N^{1/3}$ [47] and the initial size of the condensate droplet is $\sigma_0$. Particle repulsion increases the size of the condensate droplet with $N_c(T)$ particles to $\sigma(T)$. Then the potential well for normal particles $U(r)$ has a shell-type structure,

$$U(r,T) = \frac{1}{2}\hbar\omega\left[\frac{r^2}{\sigma_0^2} + \frac{N_c\sigma_0^3}{N_0\sigma^3}\exp\left(-r^2/\sigma^2\right)\right], \tag{88}$$

where $N_0 = (\sqrt{\pi}/8)\,\omega m\sigma_0^3/\hbar a_s$ and I assume that the condensate density is Gaussian with the variational parameter $\sigma$ (in Ref. [46] the shape of the condensate wave function is calculated self-consistently). The number of normal particles $N_n(T) = N - N_c(T)$ is determined from the condition $\mu = 0$. The size of the condensate droplet $\sigma(T)$ can be obtained from minimization of the condensate energy, which includes repulsion, in a way similar to Ref. [44]. There are several reasons that warrant exclusion of the interaction of normal particles *between themselves* from Eq. (88). First, for less than $10^5$ particles in a trap, the interaction of the normal particles is negligible even in the trap center before condensation. Even for larger $N$, the number of the normal particles on the *later* stages of the condensation is small. Finally, the density of the normal particles is suppressed even more by repulsion from the condensate droplet which spreads them through a large shell around the droplet $4\pi\sigma^2\sigma_0$ instead of concentrating them near the center in the volume $(4\pi/3)\,\sigma_0^3$. This gives $N$ at least an extra order of magnitude for which I can neglect the interaction of normal particles.

$N_0$ in Eq. (88) is the minimal number of particles in the condensate that is sufficient to create a strong repulsive core in the center of the trap. When $N > N_c \gg N_0$ the normal particles are pushed away from the center by the repulsive core (88) into a potential valley surrounding the condensate droplet. For Rb in a trap with $\omega = 24$ Hz, the values $a_s = 58.2$ Å, $\sigma_0 = 2.2 \times 10^{-6}$ m, and

the critical number $N_0$ that changes the topology of the normal cloud is $N_0 \approx 84$. The center of the trap becomes inaccessible for normal particles when $T$ is much smaller than the repulsion from the core. Using $T_c$ instead of $T$ and $N$ instead of $N_c$, one gets $\sigma^3 N_0/\sigma_0^3 \ll N^{2/3}$ and the critical value of $N_c$ is around $10^5$. All this means that our results are applicable for $N$ in the range $10^4 \div 10^6$.

I am able to obtain a semi-analytical description of the situation (*cf.* Refs. [45, 46]). At the later stages of the condensation, the potential (88) forms a distinct valley away from the center of the trap as soon as $N_c \gg N_0$ and equations for $N_c(T)$ and $\sigma(T)$ reduce to

$$\begin{aligned} \chi &= \sqrt{2} - \frac{\sigma_0^4}{\sqrt{2}\sigma^4} = \frac{4a_s\sigma_0^4}{\sqrt{\pi}\sigma^5} N_c, \\ N_c &= N - \sum_{n=1} \left[\exp\left[\widetilde{\beta}\left(n+\frac{1}{2}\right)\lambda\right] - 1\right]^{-1} \\ &\quad - \sum_{n,l=0} \frac{2l+1}{\exp\widetilde{\beta}\left[\left(n+\frac{1}{2}\right)\lambda + (l^2+l)\frac{\sigma_0^2}{2\sigma^2}\ln 2\chi\right] - 1} \end{aligned} \tag{89}$$

with $\widetilde{\beta} = \hbar\omega/T$, $\lambda = \sqrt{2\ln(2\chi)}$. The summation provides the temperature dependencies $N_c(T)$ and $\sigma(T)$.

I found that the condensate fraction at the later stages of condensation can be given as

$$N_c/N = 1 - (T/T_c^*)^\alpha \tag{90}$$

with a relatively high accuracy. The important feature of Eq.(90) is that the temperature is normalized not by the critical temperature $T_c$ for the onset of condensation but by a different value $T_c^*$. Since the squeezing of the normal particles towards the fringes of the trap accelerates with the number of particles in the condensate $N_c$, the normal shell narrows with increasing $N_c$, and, therefore, $N$. As a result, the effective temperature $T_c^*$ should be higher than $T_c$ and increase with increasing $N$. Dependence of $T_c^*$, or, more precisely, $T_c^*/\hbar\omega N^{1/3}$, on $N$ is presented

in Figure 15. For comparison, the critical temperature $T_c$ for non-interacting particles in a $3D$ harmonic trap is $T_c = 0.9\hbar\omega N^{1/3}$ [47]. The authors of [46], who were working with a much smaller number of particles in the trap, $N < 10^4$, did not observe any difference between $T_c$ and $T_c^*$.

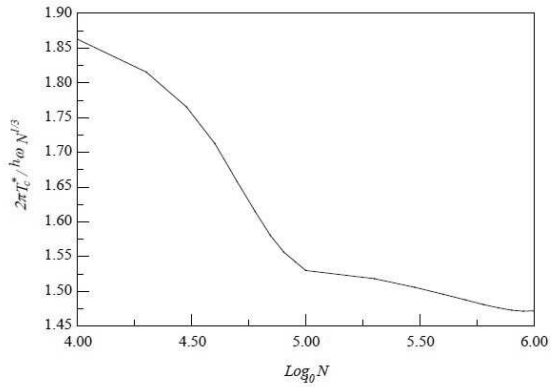


Figure 15. The reduced critical temperature, $T_c^*/\hbar\omega N^{1/3}$, w/o optical lattice

The striking change in behavior of $T_c^*(N)$ in Figure 15 occurs at $N$ for which $T_c \sim \frac{1}{2}\hbar\omega\,(N_c\sigma_0^3/N_0\sigma^3)$. At higher densities the repulsion from the condensate droplet keeps the normal particles near the bottom of the potential valley around the droplet; at lower densities, the normal particles spread out and can even reach the center of the trap. An anomaly at the same threshold density is also observed in $\alpha(N)$, Figure 16, though the index $\alpha$ remains very close to the value 2 and is practically independent of $N$, $\alpha = 2.02 \pm 1\%$, in a wide range of $N$ from $10^4$ to $10^6$. Such a weak dependence $\alpha(N)$ is surprising for a nonlinear problem of this nature. The residual temperature dependence $\alpha(T)$ lies within the same error bars.

For comparison, the same index in Ref. [46] was much higher, around 2.3, which reflects the fact that at much lower occupancy of the trap, as in [46], the

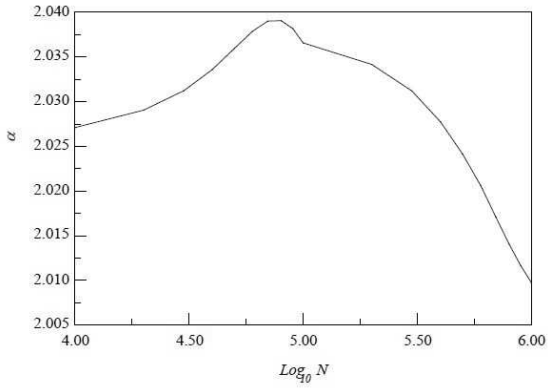


Figure 16. The density dependence of the index $\alpha$.

dimensionality of the problem is still far away from a $2D$ one. Another major difference with Ref. [46] is that we do not see any residual normal fraction, especially in the center of the trap - our condensate density is too high to allow any normal component in the center.

Our results confirm the evolution of the effective dimensionality from $3D$, for which $\alpha = 3$, to an almost perfect $2D$ value and the effective narrowing of the trap during condensation.

Using the above results as a reference point, let us turn to BEC in a trap with an optical lattice with a period $a_0$ inside. The situation with an optical lattice (Refs. [48] and references therein) inside the trap is much more complex. Here one deals with the Hubbard Hamiltonian, modified by the trap potential, and can encounter two localization effects: the localization of narrow-band particles by an inhomogeneous potential and the Mott transition [49] which requires full occupancy of the lattice sites. The latter can occur with lowering of the temperature when particles gravitate towards the bottom (center) of the trap. With sufficiently strong

on-site repulsion, the localization is practically inevitable for the condensate in the center of the trap though, of course, the Mott transition is sensitive to the trap profile [49, 50]. However, in contrast to the ground state particles, it is possible to disregard the Mott transition for the normal cloud, surrounding the condensate, due to the increased size of the condensate droplet in comparison to the system without the lattice (see below).

Condensation can be easily understood qualitatively for low initial density of particles $na_0^3 \ll 1$ and strong on-site repulsion when the condensation starts at the same temperature $T_c$ as in the absence of the interaction. The condensate forms in the center of the trap and rapidly expands in size because of the strong on-site repulsion which tends to keep the density $n_c a_0^3 \approx 1$. Though the strength of the individual particle-particle repulsion does not depend on the presence of the optical lattice, all the particles in this lattice are located in or around lattice wells and are closer to each other than when they are spread continuously throughout the trap without the lattice inside. As a result, the effect of repulsion in the trap with the lattice is stronger and the size of the condensate droplet $\sigma \sim a_0 N_c^{1/3}$ should be larger than $\sigma_{\max} \sim (2 \div 5)\,\sigma_0$ for traps without the optical lattice (Figure 17). I will not dwell on potential "freezing" of the condensate resulting from the Mott transition and will concentrate on the condensation of the normal gas outside the condensate droplet.

The main changes in our approach are associated with the band nature of the energy spectrum for particles in the optical lattice and a more complicated form of the wave functions. For the sake of comparison, in numerical computations I use a similar set of parameters: the trap potential and the particle scattering remain the same. For the particle effective mass, I use the value [42, 49] $m^* = 16m$ in most of my computations .

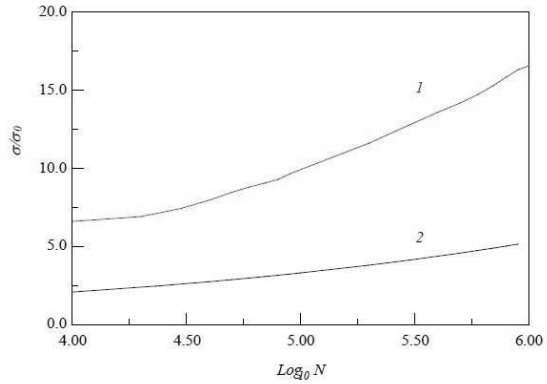


Figure 17. The condensate droplet $\sigma\left(T=0\right)$

The single-particle spectrum in the optical lattice $\epsilon\left(\mathbf{p}\right)$ has a band structure with a bandwidth $\Delta$. The effect of the trapping potential $U_{tr}\left(r\right)=\frac{1}{2}\hbar\omega\left(r/\sigma_0\right)^2$ on the particles with narrow bands results in localization of particles with energy $E=\epsilon\left(\mathbf{p}\right)+U_{tr}\left(r\right)$ in $2D$ shells $r_{\min}\leq r\leq r_{\max}$ of the thickness $\ell\left(r\right)\sim\left(\Delta/\hbar\omega\right)\sigma_0^2/r$ with $r_{\min,\max}$ given by equations $E=\pm\Delta/2+U_{tr}\left(r_{\min,\max}\right)$. An exception is the center of the trap, where the gradient of the potential is small. Since such localization suppresses the accessibility range of narrow-band particles, the density in each point contains the contributions from the particles in a finite range of energies that are localized close to this point. For example, since only the particles with very low energies, $E<\Delta$, can reach the center of the trap, the density in the center is suppressed in comparison with the trap without the optical lattice inside.

The particle wave function consists of three regions: rapid oscillations within its classically accessible shell and two attenuating tails beyond the classical turning points. The wave function $\Psi=\Psi_{lm}\left(E\right)$ for a particle with the energy $E$ decays

relatively slowly beyond the turning point $r_{\max}$ as the Airy function Ai,

$$\begin{aligned}\Psi &= B\exp\left(i\pi\left[\frac{E-\Delta/2-l\left(l+1\right)\hbar^2/2m^*d^2}{Aa}\right]\right)\\ &\times\mathrm{Ai}\left(\widetilde{r}-\frac{E-l\left(l+1\right)\hbar^2/2m^*d^2}{Aa}\right)Y_{lm}\left(\theta,\phi\right),\end{aligned}$$

and similarly near $r_{\min}$. Here $B\left(E\right)$ is the normalization coefficient, $m^*$ is the effective mass near the band minimum, $A=\hbar\omega r_{\max}/\sigma_0^2$, the dimensionless coordinate $\widetilde{r}=r/a$ has a local length scale $a=\left(\hbar^2/2m^*A\right)$, $Y_{lm}\left(\theta,\phi\right)$ are the usual angular harmonics, and $d$ is the position of the minimum of the potential (88). The spatial distribution of particles should be calculated taking into account all three regions since for relatively shallow traps the contribution from the tails of the wave function can be large. As a result, the density distribution of particles inside the trap becomes a much more complicated function of temperature than in the case without the optical lattice.

As above, I start from the situation when the particle density above condensation is low and the (Hubbard) repulsion in the normal phase is negligible. The condition of low density allows us also to disregard the Mott transition in the normal phase [51]. Since the particles in the optical lattice are located mostly on the lattice sites of the size $a_0$ rather than spread more or less uniformly, the repulsion is more effective than without the lattice. This means that the size of the condensate droplet $\sigma\left(T\right)$ should be larger than in the absence of the lattice. This is illustrated in Figure 17 which presents the ratio $\sigma\left(T=0\right)/\sigma_0$ for identical traps with (curve 1) and without (curve 2) the optical lattice. The scattering amplitude $a_s$, which is responsible for repulsion, is the same in both cases.

This seemingly innocuous lattice-driven change in the size of the condensate droplet leads to major changes in the condensation process. Even such a relatively small increase in $\sigma$ can eliminate a repulsive bump (88) in the center of the trap. Indeed, this bump disappears when $\sigma^5>\sigma_0^5\left(N_c/N_0\right)$. At these values of $\sigma$ the po-

tential (almost) restores its original parabolic structure in the central area despite the presence of the condensate. Since the value of $N$ and, therefore, $N_c$, in our calculations never exceeds $10^6$ and $N_0 \leq 100$, the potential remains parabolic for $\sigma/\sigma_0 > 10$. As a result, presence of the optical lattice strongly affects the index $\alpha$, Eq. (90), which experiences a much more noticeable change than the condensate droplet size $\sigma$, Figure 18. This density dependence $\alpha(N)$ is dramatically different from the one in Figure 16 for the trap without the optical lattice inside.

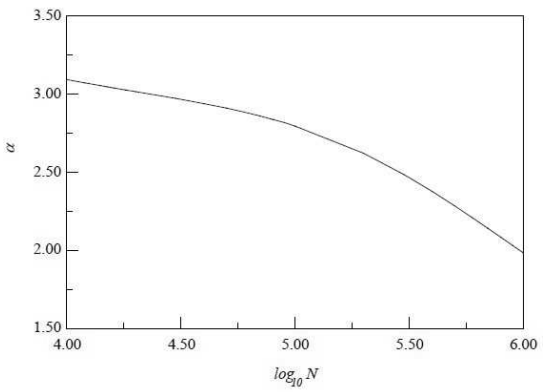


Figure 18. Index $\alpha$ with optical lattice.

In Fig. 18, $\alpha$ starts from a $3D$ value at small density of particles which is understandable since there is no repulsive core in the center. With increasing number of particles the size of the condensate droplet grows leaving fewer normal particles in the central area and gradually reducing $\alpha$ to its quasi-$2D$ value. What is not clear is why does $\alpha$ continue to decline with a further increase in $N$; however, since our approach loses accuracy beyond $N \sim 10^6$, I do not present these data in this figure. Note, that if one also plots in Figure 18 the curve $\alpha(N)$ for a system without the optical lattice from Figure 16, all its residual dependence on

$N$ becomes invisible in the scale of Figure 16. This difference in dependences of the index $\alpha$ on the number of trapped particles between Figure 16 and 18 is due mostly to the major qualitative changes in the wave functions imposed by the lattice symmetry. Computations with a smaller effective mass did not lead to any major changes in behavior of $\alpha\,(N)$.

In general, the decrease in $\alpha\,(N)$ is accompanied by an increase in $T_c^*\,(N)$, which in the presence of the optical lattice grows much faster than the $N^{1/3}$-dependence inherent to a free gas in a trap, Figure 19.

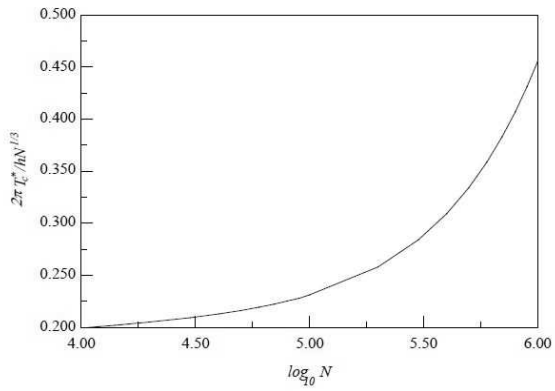


Figure 19. The reduced critical temperature $T_c^*/\hbar\omega N^{1/3}$ with optical lattice.

### 1.3.1 Summary of competing phenomena in a trapped BEC

In summary, I calculated the index for a temperature dependence of the condensate fraction for interacting gas inside harmonic trap. The results for traps without the optical lattice inside are quite clear: the repulsion from the condensate droplet pushes normal particles away from the center of the trap and concentrates them in a relatively thin shell around this droplet. Then the condensation becomes almost quasi-$2D$ with the index $\alpha \approx 2$. The presence of the optical lattice inside

the trap changes the situation in a major way. The index $\alpha$ acquires a strong dependence on the number of particles inside the trap and gradually falls from a $3D$ to a $2D$ value with an increase in the number of particles. This change in the index, which is caused by the presence of the optical lattice, is explained by the wider spread of the condensate droplet and the localization of the narrow band particles by the trap potential.

## 1.4 Conclusion

In my investigations on restricted systems where competing phenomena influence the underlying physics of some key properties of the systems, I have found that when these competing "forces" or "channels" are of the same order of magnitude, they often do not act independent of each other. Instead, the effect of one "channel" reinforces that of the other and the interference effects due to the two channels become significant and are measurable. My study shows that in such situations it is important to have a common mathematical framework that treats all the competing phenomena in the same manner so that interference effects can be studied without the obfuscating presence of mathematical artifacts, which are the usual side effect when one is not able to treat the different phenomena in a common framework. In keeping with this principle, I have used a collision operator (first proposed in Ref. [16] ) that incorporates both surface roughness scattering and bulk impurity scattering in order to investigate non-Matthiessen terms in the resistivity of thin films. When the films are so thin that the scattering due to the surface roughness becomes comparable or even stronger than that due to the bulk impurities, I found that one had to be careful in not neglecting the interference between the two channels. The Matthiessen's rule of independent scattering by the two channels was seen to break down and the interference terms were shown to have a nontrivial dependence on the temperature, bulk mean free path and the

amplitude and correlation length of the surface roughness. I derived simple analytical expressions for these dependencies for large bulk free paths $\mathcal{L}_b$ and large correlation radii (lateral sizes) $R$ of surface inhomogeneities that can be used by experimentalists investigating the same phenomena. When the bulk scattering and the surface roughness scattering became such that the condition, $R^2 \sim a\mathcal{L}_b$, was satisfied, a crossover could be predicted between two asymptotic regimes for the interference contributions characterized by a different dependence to temperature and concentration.

Then I studied a different restricted system: a strongly interacting trapped BEC in an optical lattice. In my study of these systems, I focussed primarily on investigating how the strong particle interactions which have a widening effect on the condensate droplet competes against the confining nature of the trap while the BEC is made to lie in an optical lattice which causes the particle wave functions to be Airy functions along the walls of the trap. As an application of the general principle of having a self-consistent common framework to describe all the competing effects, I used a physical model that can describe the competing effects of particle interactions and a trap on a BEC in a self-consistent way and derived important parameters of condensation. I calculated the index for a temperature dependence of the condensate fraction for the interacting gas inside the harmonic trap and found that it falls from a $3D$ to a $2D$ value with an increase in the number of condensate particles. This change in the index, which is caused by the presence of the optical lattice, is explained by the wider spread of the condensate droplet and the localization of the narrow band particles by the trap potential.

**List of References**

[1] J. J. Plombon, E. Andideh, V. M. Bubin, and J. Maiz, *Journal of Applied Physics Letters*, vol. 89, p. 113124, 2006.

[2] E. Sondheimer, *Advances In Physics*, vol. 1, p. 1, 1952.

[3] J. R. Sambles, *Thin Solid Films*, vol. 106, p. 321, 1983.

[4] K. Fuchs, *Proceedings of Cambridge Philosophical Society*, vol. 34, p. 100, 1938.

[5] Z. Tesanovic, *Journal of Physics C: Solid States Physics Letters*, vol. 20, p. L289, 1987.

[6] Y. Namba, *Japanese Journal of Applied Physics*, vol. 9, p. 1376, 1970.

[7] Z. Tesanovic, M. V. Jaric, and S. Maekawa, *Physical Review Letters*, vol. 57, p. 2760, 1986.

[8] N. Trivedi and N. W. Aschroft, *Physical Review B*, vol. 38, p. 12298, 1988.

[9] A. E. Meyerovich and S. Stepaniants, *Physical Review Letters*, vol. 73, p. 316, 1994.

[10] A. E. Meyerovich and A. Stepaniants, *Physical Review B*, vol. 60, p. 9129, 1999.

[11] A. E. Meyerovich and A. Stepaniants, *Physical Review B*, vol. 58, p. 13242, 1998.

[12] G.Fishman and D.Calecki, *Physical Review Letters*, vol. 62, p. 1302, 1989.

[13] L. Sheng, D. Y. Xing, and Z. D. Wang, *Physical Review B*, vol. 51, p. 7325, 1995.

[14] R. C. Munoz, G. Vidal, G. Kremer, L. Moraga, and C. Arenas, *Journal of Physics: Condensed Matter*, vol. 11, p. L299, 1999.

[15] R. C. Munoz, R. Finger, C. Arenas, G. Kremer, and L. Moraga, *Physical Review B*, vol. 66, p. 205401, 2002.

[16] A. E. Meyerovich and A. Stepaniants, *Journal of Physics: Condensed Matter*, vol. 12, p. 5575, 2000.

[17] J.A.Ogilvy, *Theory of Wave Scattering from Random Surfaces.* Adam Hilger, Bristol, 1991.

[18] R. M. Feenstra, D. A. Collins, D. Z.-Y. Ting, M. W. Wang, and T. C. McGill, *Physical Review Letters*, vol. 72, p. 2749, 1994.

[19] G. V. R. C. Munoz, G. Kremer, L. Moraga, C. Arenas, and A. Concha, *Journal of Physics: Condensed Matter*, vol. 12, p. 2903, 2000.

[20] A. E. Meyerovich and I. V. Ponomarev, *Physical Review B*, vol. 65, p. 155413, 2002.

[21] Y. Cheng and A. E. Meyerovich, *Physical Review B*, vol. 73, p. 085404, 2006.

[22] A. A. Abrikosov, *Fundamentals of the Theory of Metals*, North Holland, Amsterdam, 1988.

[23] G. Grimvall, *The Electron/Phonon Interaction in Metals*, Elsevier, Amsterdam, 1981.

[24] G. Kastle, H.-G. Boyen, A. Schroder, A. Plettl, and P. Ziemann, *Physical Review B*, vol. 70, p. 165414, 2004.

[25] V.B.Sandomirskii, *Soviet Physics-JETP*, vol. 25, p. 101, 1967.

[26] G. Fischer and H. Hoffmann, *Solid State Communications*, vol. 35, p. 793, 1980.

[27] L. A. Kuzik, Y. E. Petrov, F. A. Pudonin, and V. A. Yakovlev, *Soviet Physics - JETP*, vol. 78, p. 114, 1994.

[28] A. E. Meyerovich, *Journal of Low Temperature Physics*, vol. 124, p. 461, 2001.

[29] R. M. Bowley and K. A. Benedict, *Journal of Low Temperature Physics*, vol. 142, p. 701, 2006.

[30] B. Feldman, R. Deng, and S. Dunham, *Journal of Applied Physics*, vol. 103, p. 113715, 2008.

[31] A. E. Meierovich and B. E. Meierovich, *Soviet Physics - JETP*, vol. 66, p. 833, 1987.

[32] A. E. Meyerovich and D. Chen, *Physical Review B*, vol. 66, p. 235306, 2002.

[33] J.Rammer and H.Smith, *Review of Modern Physics*, vol. 58, p. 323, 1986.

[34] R. C. Munoz, C. Arenas, G. Kremer, and L. Moraga, *Journal of Physics Condensed Matter*, vol. 15, p. L177, 2003.

[35] H. Marom and M. Eizenberg, *Journal of Applied Physics*, vol. 99, p. 123705, 2006.

[36] J. M. Purswani and D. Gall, *Thin Solid Films*, vol. 516, p. 465, 2007.

[37] V.B.Sandomirskii, *Soviet Physics - JETP*, vol. 25, p. 101, 1967.

[38] S. Chatterjee and A. E. Meyerovich, *Physical Review B*, vol. 81, p. 245409, 2010.

[39] E. A. Cornell and C. E. Wieman, *Review of Modern Physics*, vol. 74, p. 875, 2002.

[40] A. J. Leggett, *Review of Modern Physics*, vol. 73, p. 307, 2001.

[41] H. J. Lewandowski, D. M. Harber, D. L. Whitaker, and E. A. Cornell, *Physical Review Letters*, vol. 88, p. 070403, 2002.

[42] M. Greiner, O. Mandel, T. W. Hansch, and I. Blochl, *Nature*, vol. 415, p. 39, 2002.

[43] V. A. Kashurnikov, N. V. Prokof'ev, and B. Svistunov, *Physical Review Letters*, vol. 92, p. 050402, 2004.

[44] G. Baym and C. J. Pethick, *Physical Review Letters*, vol. 76, p. 6, 1996.

[45] S. Giorgini, L. P. Pitaevskii, and S. Stringari, *Physical Review A*, vol. 54, p. R4633, 1996.

[46] D. A. W. Hutchinson, E. Zaremba, and A. Griffin, *Physical Review Letters*, vol. 78, p. 1842, 1997.

[47] V. V. Goldman, I. F. Silvera, and A. J. Leggett, *Physical Review B*, vol. 24, p. 2870, 1981.

[48] G. Raithel, G. Birkl, A. Kastberg, W. D. Phillips, and S. L. Rolston, *Physical Review Letters*, vol. 78, p. 630, 1997.

[49] D. Jaksch, C. Bruder, J. I. Cirac, C. W. Gardiner, and P. Zoller, *Physical Review Letters*, vol. 81, p. 3108, 1998.

[50] G. K. Campbell, J. Mun, M. Boyd, P. Medley, A. E. Leanhardt, L. G. Marcassa, D. E. Pritchard, and W. Ketterle, *Science*, vol. 313, p. 649, 2006.

[51] A. E. Meyerovich, *Physical Review A*, vol. 68, p. 051602(R), 2003.

## BIBLIOGRAPHY


Abrikosov, A. A., *Fundamentals of the Theory of Metals*, North Holland, Amsterdam, 1988.

Baym, G. and Pethick, C. J., *Physical Review Letters*, vol. 76, p. 6, 1996.

Bowley, R. M. and Benedict, K. A., *Journal of Low Temperature Physics*, vol. 142, p. 701, 2006.

Campbell, G. K., Mun, J., Boyd, M., Medley, P., Leanhardt, A. E., Marcassa, L. G., Pritchard, D. E., and Ketterle, W., *Science*, vol. 313, p. 649, 2006.

Chatterjee, S. and Meyerovich, A. E., *Physical Review B*, vol. 81, p. 245409, 2010.

Cheng, Y. and Meyerovich, A. E., *Physical Review B*, vol. 73, p. 085404, 2006.

Cornell, E. A. and Wieman, C. E., *Review of Modern Physics*, vol. 74, p. 875, 2002.

Feenstra, R. M., Collins, D. A., Ting, D. Z.-Y., Wang, M. W., and McGill, T. C., *Physical Review Letters*, vol. 72, p. 2749, 1994.

Feldman, B., Deng, R., and Dunham, S., *Journal of Applied Physics*, vol. 103, p. 113715, 2008.

Fischer, G. and Hoffmann, H., *Solid State Communications*, vol. 35, p. 793, 1980.

Fuchs, K., *Proceedings of Cambridge Philosophical Society*, vol. 34, p. 100, 1938.

G.Fishman and D.Calecki, *Physical Review Letters*, vol. 62, p. 1302, 1989.

Giorgini, S., Pitaevskii, L. P., and Stringari, S., *Physical Review A*, vol. 54, p. R4633, 1996.

Goldman, V. V., Silvera, I. F., and Leggett, A. J., *Physical Review B*, vol. 24, p. 2870, 1981.

Greiner, M., Mandel, O., Hansch, T. W., and Blochl, I., *Nature*, vol. 415, p. 39, 2002.

Grimvall, G., *The Electron/Phonon Interaction in Metals*, Elsevier, Amsterdam, 1981.

Hutchinson, D. A. W., Zaremba, E., and Griffin, A., *Physical Review Letters*, vol. 78, p. 1842, 1997.

Jaksch, D., Bruder, C., Cirac, J. I., Gardiner, C. W., and Zoller, P., *Physical Review Letters*, vol. 81, p. 3108, 1998.

J.A.Ogilvy, *Theory of Wave Scattering from Random Surfaces*. Adam Hilger, Bristol, 1991.

J.Rammer and H.Smith, *Review of Modern Physics*, vol. 58, p. 323, 1986.

Kashurnikov, V. A., Prokof'ev, N. V., and Svistunov, B., *Physical Review Letters*, vol. 92, p. 050402, 2004.

Kastle, G., Boyen, H.-G., Schroder, A., Plettl, A., and Ziemann, P., *Physical Review B*, vol. 70, p. 165414, 2004.

Kuzik, L. A., Petrov, Y. E., Pudonin, F. A., and Yakovlev, V. A., *Soviet Physics - JETP*, vol. 78, p. 114, 1994.

Leggett, A. J., *Review of Modern Physics*, vol. 73, p. 307, 2001.

Lewandowski, H. J., Harber, D. M., Whitaker, D. L., and Cornell, E. A., *Physical Review Letters*, vol. 88, p. 070403, 2002.

Marom, H. and Eizenberg, M., *Journal of Applied Physics*, vol. 99, p. 123705, 2006.

Meierovich, A. E. and Meierovich, B. E., *Soviet Physics - JETP*, vol. 66, p. 833, 1987.

Meyerovich, A. E., *Journal of Low Temperature Physics*, vol. 124, p. 461, 2001.

Meyerovich, A. E., *Physical Review A*, vol. 68, p. 051602(R), 2003.

Meyerovich, A. E. and Chen, D., *Physical Review B*, vol. 66, p. 235306, 2002.

Meyerovich, A. E. and Ponomarev, I. V., *Physical Review B*, vol. 65, p. 155413, 2002.

Meyerovich, A. E. and Stepaniants, A., *Physical Review B*, vol. 58, p. 13242, 1998.

Meyerovich, A. E. and Stepaniants, A., *Physical Review B*, vol. 60, p. 9129, 1999.

Meyerovich, A. E. and Stepaniants, A., *Journal of Physics: Condensed Matter*, vol. 12, p. 5575, 2000.

Meyerovich, A. E. and Stepaniants, S., *Physical Review Letters*, vol. 73, p. 316, 1994.

Munoz, R. C., Arenas, C., Kremer, G., and Moraga, L., *Journal of Physics Condensed Matter*, vol. 15, p. L177, 2003.

Munoz, R. C., Finger, R., Arenas, C., Kremer, G., and Moraga, L., *Physical Review B*, vol. 66, p. 205401, 2002.

Munoz, R. C., Vidal, G., Kremer, G., Moraga, L., and Arenas, C., *Journal of Physics: Condensed Matter*, vol. 11, p. L299, 1999.

Namba, Y., *Japanese Journal of Applied Physics*, vol. 9, p. 1376, 1970.

Plombon, J. J., Andideh, E., Bubin, V. M., and Maiz, J., *Journal of Applied Physics Letters*, vol. 89, p. 113124, 2006.

Purswani, J. M. and Gall, D., *Thin Solid Films*, vol. 516, p. 465, 2007.

R. C. Munoz, G. V., Kremer, G., Moraga, L., Arenas, C., and Concha, A., *Journal of Physics: Condensed Matter*, vol. 12, p. 2903, 2000.

Raithel, G., Birkl, G., Kastberg, A., Phillips, W. D., and Rolston, S. L., *Physical Review Letters*, vol. 78, p. 630, 1997.

Sambles, J. R., *Thin Solid Films*, vol. 106, p. 321, 1983.

Sheng, L., Xing, D. Y., and Wang, Z. D., *Physical Review B*, vol. 51, p. 7325, 1995.

Sondheimer, E., *Advances In Physics*, vol. 1, p. 1, 1952.

Tesanovic, Z., *Journal of Physics C: Solid States Physics Letters*, vol. 20, p. L289, 1987.

Tesanovic, Z., Jaric, M. V., and Maekawa, S., *Physical Review Letters*, vol. 57, p. 2760, 1986.

Trivedi, N. and Aschroft, N. W., *Physical Review B*, vol. 38, p. 12298, 1988.

V.B.Sandomirskii, *Soviet Physics-JETP*, vol. 25, p. 101, 1967.

V.B.Sandomirskii, *Soviet Physics - JETP*, vol. 25, p. 101, 1967.